LR - 655

BULGING OF FATIGUE CRACKS IN A PRESSURIZED AIRCRAFT FUSELAGE

May 1991

D. Chen and J. Schijve

TU Delft
Delft University of Technology

Faculty of Aerospace Engineering

BULGING OF FATIGUE CRACKS IN A PRESSURIZED AIRCRAFT FUSELAGE

D. Chen and J. Schijve

BULGING OF FATIGUE CRACKS IN A PRESSURIZED AIRCRAFT FUSELAGE

D.Chen and J.Schijve

Paper presented at the 16th ICAF Symposium, Tokyo, 22-24 May 1991

Fatigue crack growth and residual strength must be considered as part of the damage problem of a pressurized aircraft fuselage. Longitudinal cracks offer problems because they occur in a curved thin sheet structure under biaxial loading conditions and internal pressure. The fatigue crack edges bulge outwards (out-of-plane deformation) which considerably complicates the fracture mechanics analysis. The problem is analyzed empirically and theoretically. Three test set-ups were developed respectively for (1) sheet specimens under biaxial loading, (2) tensile loading of curved sheet specimens, and (3) sheet specimens with a large radius of curvature loaded by internal air pressure and hoop stress. Fatigue crack growth and residual strength tests were carried out on aluminium alloy sheet specimens and some panels of new metal-sheet/fibre laminates (ARALL and GLARE). Analytical relations were developed to obtain K-values, which account for the non-linear behaviour associated with sheet curvature and bulging-out of the crack edges. The predictions agree with the present test results, and with results from the literature obtained by FEM calculations for fuselages and in full-scale fatigue tests.

INTRODUCTION

Fatigue cracks in aircraft fuselages have been a significant safety problem since the introduction of the pressurized passenger cabin. Several catastrophic decompression failures have occurred in service (1). The most well known failures are the accidents of two Comet aircraft in the early fifties. The Aloha accident in 1988 is another noteworthy case in view of multiple-site damage in aging aircraft. In full-scale fatigue tests unstable crack extension has also been observed.

The problem of fatigue cracks in pressurized fuselages is still relevant in these days, because aircraft are used longer and more intensively, and stress levels have been increased for weight saving. The growth rate of fatigue cracks and the effect of cracks on the residual strength must be considered as part of the airworthiness certification. Nowadays fracture mechanics is used for that purpose. Some years ago an interesting analysis of the Comet accidents was given by Swift (2), based on concepts of fracture mechanics.

The problem of longitudinal cracks in a pressurized aircraft fuselage is characterized by specific aspects:

- The crack does not occur in a flat sheet, but in a *curved* thin sheet structure.
- The conditions are *biaxial* and not uniaxial, and at the same time there is an internal pressure.
- The *crack edges bulge outwards* (out of plane deformation), which considerably complicates the fracture mechanics analysis.

Information in the literature on the analysis of cracks in thin sheet pressurized fuselages is fairly limited. In the present paper it is tried to analyze the subject problem empirically and theoretically. For that purpose three test set-ups were developed:

(1) a specimen configuration to load sheet specimens under biaxial conditions,
(2) a test set-up for tensile loading of curved sheet specimens, and
(3) another test set-up for specimens with a large radius of curvature loaded by internal air pressure and hoop stress.

Fatigue crack growth and residual strength tests were carried out on aluminium alloy sheet specimens of 2024-T3 and 7075-T6. The problem of fatigue cracks in fuselages can also be solved by developing new fatigue resistant materials, which is now done in the Materials & Structures Laboratory of the Faculty of Aerospace Engineering in Delft. Some exploratory tests have been carried out on ARALL laminates (aramid aluminium laminates) and GLARE (glass fibre aluminium laminates. Results for these new materials will also be presented.

Analytical relations have been developed based on fracture mechanics to obtain K-values, which account for the non-linear behaviour associated with sheet curvature, biaxial conditions, and bulging-out of the crack edges. The predictions are compared with the present test results, and with results from the literature obtained by FEM calculations for fuselages and in full-scale fatigue tests.

EXPERIMENTAL DETAILS

Specimen for biaxial loading (SUPERBAT)

The cruciform specimen is a classical one for biaxial loading of sheet material. The major problem is the introduction of the biaxial loads on the central test section, because fatigue crack initiation outside the test section must be avoided. Recently, the National Aerospace Laboratory NLR developed an interesting load transmission (3) by employing uni-directional composite laminates for that purpose. This solution is not so easily applicable on curved sheet specimens. Moreover, it requires a biaxial testing machine, which is not available in our laboratory. We have chosen for a limited amount of biaxiality obtained by preventing the Poisson contraction. If the contraction can be fully prevented, the biaxiality ratio:

$$\chi = \frac{\sigma_x}{\sigma_y} \qquad (1)$$

(y = main loading direction, x = transverse direction, direction of crack growth) easily follows from:

$$\varepsilon_x = \frac{\sigma_x}{E} - \nu\frac{\sigma_y}{E} = 0 \qquad (2)$$

which gives $\chi = \nu$. For aluminium alloys $\nu = 0.33$. For an unstiffened pressure vessel χ = (longitudinal stress/hoop stress) = 0.5. In an aircraft fuselage, however, longitudinal stiffeners (longerons) are present. As a consequence, the biaxiality induced by the pressurization is lower. It may be in the order of 0.4, although locally it can be substantially higher, e.g. in the crown section due to fuselage bending.

The Poisson contraction was restrained in the test section of the specimen by mounting four transverse steel bars on both sides of the sheet specimen, see Figure 1. The biaxiality in the test section was both calculated and measured with strain gages. The agreement between calculations and measurements was quite good. The biaxiality ratio obtained was 0.24 on Al-alloy specimens and 0.28 on ARALL specimens. That value is not as high as desirable, but it turned out to be high enough for a significant effect on crack edge bulging. The specimen is referred to as the SUPERBAT specimen (Specimen Using Poisson Ratio Effect for Bi-Axial Testing).

Test set-up for curved specimens (CETS)

An experimental set-up has been designed to investigate the fracture behaviour of thin Al-alloy sheet specimens under combined tension and bending loads (CETS: Curvature Effect Testing System). An originally flat sheet is forced to take a predetermined curvature by placing the sheet between a curved block and two press rolls, see Figure 2. To reduce the friction force, thin teflon films are fixed between the specimen and the rolls and the block. Four blocks with different radii were made, viz. with ρ = 130, 375, 750 and 1500 mm respectively. It should be realized that a specimen loaded in this test set up is subjected to a constant bending deformation (dictated by the radius of curvature ρ), and an increasing tensile load (static test) or a cyclic tensile load (fatigue test).

Test set-up for curved sheet specimens loaded under internal pressure and hoop stress conditions

The test set-up (PFSTS = Pressurized Fuselage Skin Test System), see Figure 3, consists of a pressurization chamber, which at one side is closed by a bent specimen, length 1080 mm, width 500 mm. The standard radius of curvature is 2000 mm, but smaller radii can be adopted by changing wedges of the specimen clampings. The internal pressure can be varied between 0 and 2.5 bar for both static and cyclic loading conditions. The maximum pressure of 2.5 bar is obviously far in excess of the maximum cabin pressure of an aircraft.

The sealing of the system is realized by a plastic foil covering the whole

inner side of the specimen including the grips. Because of the very small stiffness of the plastic foil compared to the specimen, the sealing itself does not take any pressure load during the test. For a fatigue test, a cut-out is made in the plastic foil at the location of the crack to allow a free air flow through the crack. The plastic foil is then sealed around the crack. The air flow through the crack produces a considerable noise. Therefore, the test set-up was placed in the basement of the laboratory.

A home built pressure control system was built, which includes an air reservoir, a pressure controller and several valves and pressure gages. The pressure chamber was filled for about 90% with wood, in order to reduce the volume of the compartment for increasing the test frequency. Cyclic periods of 4 seconds (0.25 Hz) could be obtained. Strain gages indicated a very good agreement between the measured and calculated hoop stress ($\sigma_{hoop} = p\rho/t$). Small bending deformations at the grips were found to have a negligible influence on the stresses at the centre of the specimen.

The SUPERBAT specimen can also be used in the PFSTS set-up, which allowes observations of the biaxiality effect on crack edge bulging and fatigue crack growth.

TEST PROGRAM AND RESULTS

Fatigue tests on SUPERBAT specimens (biaxial loading)

Fatigue tests were carried out on sheet specimens of 2024-T3 Alclad (1.2 mm) and bare 7075-T6 (1.6 mm). Specimen width 300 mm, length 500 mm. Constant-amplitude tests were carried out at σ_{max} = 100 MPa, σ_{min} = 0 (R = 0) and a frequency of 10 Hz. Two similar tests were carried out for each test condition. The results for 7075-T6 are shown in Figure 4, which indicates no effect of the biaxiality (χ = 0.24). Also for 2024-T3 all results were in a narrow scatter band with no obvious effect of biaxiality.

The absence of a biaxiality effect is generally confirmed in the literature, although there are some indications that such an effect may be present for high K_{max}-values (4,5). It is then associated with an effect on the size and the shape of the plastic zone and an effect of crack closure. For the stress levels in aircraft fuselages a significant effect should not be expected.

Residual static strength tests under combined tension and bending (CETS)

Bare thin sheet material of the two alloys 2024-T3 and 7075-T6 with two thicknesses (0.5 and 1.0 mm) was used for each alloy. The specimen dimension were: width 160 mm, length 500 mm. Four curvature radii were used, viz. 130, 375, 750 and 1500 mm. In addition flat specimens were also tested. Initial cracks were simulated with narrow saw cuts (width 0.3 mm) with four different lengths: a = 10, 20, 30 and 40 mm (2a/W = 0.125, 0.25, 0.375 and 0.5 respectively). The results are presented in Figure 5 as the critical gross stress at specimen failure. A systematic curvature effect was apparently found, i.e. the residual strength

decreases if the radius of curvature becomes smaller. The effect is fairly small for t = 0.5 mm, but it is larger for t = 1.0 mm. Almost linear residual strength curves parallel to the net-section yield line are found for the 2024-T3 specimens. The flat 2024-T3 specimens confirmed the net-section yield behaviour, whereas the flat 7075-T6 specimens indicate a K_c = 73 MPa$\sqrt{m}$ for t = 1.0 mm and K_c = 72 MPa$\sqrt{m}$ for t = 0.5 mm (practically similar values).

Fatigue crack growth tests under combined tension and bending were carried out with the same test set up. For t = 1 mm the smallest radius (ρ = 130 mm) could not be used, but for t = 0,5 mm tests with all four radii were carried out. In general the effect of the curvature was practically absent. Only for the smallest radius (ρ = 130 mm) a slightly smaller crack growth rate was found. Figure 6 shows the results for the lowest radius and for a flat specimen. The results for ρ = 375, 750 and 1500 mm did not systematically differ from the results for the flat specimen. It should be noted from Fig.6 that the crack growth results for ρ = 130 mm are slightly lower than for a flat sheet (and for the larger radii), which implies a favourable effect of the curvature instead of an unfavourable effect.

Pressurized fuselage skin tests on 2024-T3 Alclad

Fatigue tests were carried out on sheet specimens of 2024-T3 Alclad (1.2 mm). The specimen size had to be adapted to the pressurized fuselage skin test system (PFSTS) described before. It implies a specimen width of 500 mm and a length of 1080 mm. The radius of curvature is 2000 mm. Specimens with restrained lateral contraction (SUPERBAT specimen, see Fig.1) were also tested. The biaxiality ratio obtained was χ = 0.24.

Tests were carried out at two different pressure levels, viz. p = 0.35 bar and p = 0.55 bar, which are representative for cruising altitudes of 6000 and 10000 m respectively. For χ = 0.24 the pressure levels were just slightly higher (i.e. 0.36 and 0.56 bar) due to a modification of the pressure sensor.

An example of test results is given in Figure 7 (= 5.21a). In general two similar tests were carried out for each test condition. The crack growth rate as a function of the crack length is presented in Figures 8a and 8b. Scatter between two similar tests was very low. The average da/dN curves as a function of ΔK are shown in Figure 9, including the average curve for flat specimens of the same size. Some trends can easily be observed in this graph:

- The crack growth rate is larger for the curved pressurized specimens than for the flat specimens. There is an unfavourable effect.
- The crack growth rate as a function of the nominal ΔK is larger for a higher air pressure.
- The crack growth rate is lower for biaxially loaded specimens than for uniaxially loaded specimens. The biaxiality has a favourable effect.

During the tests crack edge bulging (out of plane deformation) could easily be observed. The out of plane deformations were measured by scanning the sheet surface with an LVDT (displacement transducer). Records were made by moving the transducer along lines parallel to the crack (y = constant) at several

distances to the crack. An example of the deformation field obtained is shown in Figure 10. Such measurements were made at different pressure levels (0.3, 0.4 and 0.55 bar) and for six different values of the crack length (25 to 50 mm). The non-linear behaviour of the bulge out phenomenon is illustrated by the results in Figure 11, which shows the maximum crack edge displacement w_o (at x = 0, y = 0) as a function of the applied internal pressure.

The out-of-plane deformations of a biaxially loaded specimen could not be measured in the same way. The steel strips (Fig.1), which prevent the lateral Poisson contraction, also obstruct a scanning with the displacement transducer. However, it was evident from visual observations that bulging out of the crack edges was substantially reduced under the biaxial conditions.

The application of fracture mechanics on fatigue cracks becomes problematic when crack edge bulging occurs. As part of the present study a bulge factor has been adopted, defined by:

$$\beta_b = \frac{K_{bulge}}{K_{flat}} \tag{3}$$

The stress intensity factor K_{bulge} applies to the pressurized fuselage where bulging occurs. K_{flat} applies to a flat sheet specimen of the same material and thickness, and similar geometrical conditions. For the present specimens it implies the same crack length, and K_{flat} is then obtained with the Feddersen width correction factor as:

$$K_{flat} = \sigma\sqrt{\pi a \sec(\pi a/W)} \tag{4}$$

For the pressurized specimens K_{bulge} was obtained empirically by adopting the similarity approach. It says that similar crack growth rates should be associated with the same ΔK ranges if the same stress ratio R is applicable. For a flat sheet specimen the material data are represented by:

$$da/dN = f(\Delta K, R) \tag{5}$$

which can be used in an analytical format (e.g. the Forman equation) or in graphical shape. K_{bulge} is now obtained by substituting the da/dN of the pressurized specimen into Eq.(5). As an example the results of Figure 7 converted into $\beta_b(a)$ are presented in Figure 12.

ANALYSIS OF THE RESULTS

Tests on curved specimens, no internal pressure (CETS)

The residual strength tests showed that the results of the curved 2024-T3 sheet specimens (Fig.5) might be associated with net section yield behaviour. A fracture mechanics prediction based on K_{Ic} (or K_c) should then be unsuccessful. However, for the 7075-T6 sheet material failure occurred at a stress level considerably below the net section yield level. In (1) several approaches for predicting the behaviour were considered. The following one was most successful.
Failure is supposed to occur if:

$$K_{I,e} + K_{I,b} = K_{Ic} \tag{6}$$

(e for extension, b for bending). The bending K factor is obtained from:

$$K_{I,b}^2 = \frac{E G_b}{t} \tag{7}$$

with

$$G_b = \lim_{\alpha \to 1} \frac{2}{\alpha} \int_{-\frac{t}{2}}^{\frac{t}{2}} \int_0^{\alpha} \frac{\sigma_{yy} u_y}{2} \, dx \, dz \tag{8}$$

For the last equation it is assumed that the crack under bending is still kept open by the tensile load. The equations imply that the strain energy release rate is averaged over the sheet thickness. A further evaluation of Eq.(8) and substitution in Eq.(7) leads to:

$$K_{I,b} = \frac{1}{\sqrt{3}} \frac{1-\nu}{3+\nu} \sigma_b \sqrt{\pi a} \tag{9}$$

where σ_b is the bending stress induced by the curvature (radius = ρ). Combining of Eqs.(6) and (9) leads to the residual strength equation:

$$\sigma_e = \sigma_c - \frac{1}{\sqrt{3}} \frac{1+\nu}{3+\nu} \sigma_b \tag{10}$$

where σ_c is the residual strength if there is no bending. For a specific value of ρ the bending stress (σ_b) is constant. Eq.(10) then implies that the residual strength is reduced by a constant stress decrement depending on the radius ρ. The largest reduction is obtained for ρ = 130 mm. Results for this radius (Fig.13) show that the predicted Feddersen diagrams are very satisfactory. Equally satisfactory predictions were obtained for the other larger ρ-values. The more remarkable finding is that the predictions are also very good for the ductile 2024-T3 alloy.

The fatigue tests indicated a slightly slower crack growth for the smallest radius of curvature (ρ = 130 mm), see Figure 6. This is attributed to *partial crack closure*. Figure 14 indicates that the cyclic stress at the inner side of the sheet is partly compressive, and thus will close the crack. The effective stress range, averaged over the sheet thickness will be smaller than the nominal average value. As a result a lower crack growth rate is obtained. This picture is a simplification of the actual situation in view of the simultaneously occurring crack closure induced by plastic deformation (Elber mechanism). Nevertheless, partial crack closure due to bending is qualitatively a plausible explanation for the observed trend. For radii representative for aircraft fuselages, however, the bending effect can be ignored.

Tests on curved, pressurized specimens

As mentioned previously, bulging of a cracked unstiffened thin-walled cylinder is a non-linear problem, which can not easily be analyzed by the classical theory of elasticity. It has been tried in (1) to arrive at an approximate K-factor by adopting the energy balance approach, which will be summarized here. The energy release rate can be defined as:

$$G = \frac{d}{da}(F - U) \tag{11}$$

where F is the work done by external forces and U the change of the elastic strain energy, both related to an incremental crack extension. Exact solution can not be given, but approximate values can be obtained by simplifying the geometry of the bulged crack configuration. One half of the bulged area is drawn in Figure 15. The geometry is now approximated by assuming that the bulge deformation can be represented by the pyramidal shape ABCD with the characteristic dimensions s_1, s_2 and w_o (out-of-plane displacement at point A). It should be noted that s_2 is always larger than the crack length a.

The consequence of bulging on Eq.(11) is that F and U should include parts related to bulging. It can be written as:

$$G = \frac{d}{da}(F_{cyl.} - U_{cyl.} + F_{bulge} - U_{bulge}) \tag{12}$$

The term (F_{bulge} - U_{bulge}) is the additional energy available for the crack extension da, which is responsible for the increase of the stress intensity factor as compared to K for the unbulged cylinder. The increment dF_{bulge} is the work done by the internal pressure p. With the pyramidal approximation it follows that:

$$dF_{bulge} \approx 4p\, d(\text{volume of pyramid ABCD}) - \frac{2}{3} p\, d(s_1 s_2 w_o) \qquad (13)$$

Because $w_o << s_1, s_2$:

$$dF_{bulge} \approx \frac{2}{3} p\, s_1\, s_2\, dw_o \qquad (14)$$

dU_{bulge} can be estimated by adopting the analogy with the well known "fixed load" problem of a flat panel. It implies that $dU_{bulge} = \frac{1}{2}\, dF_{bulge}$. The analogy is not fully justified in view of the non-linear behaviour, but the error made will be relatively small. As a result:

$$dF_{bulge} - dU_{bulge} \approx \frac{1}{3} p\, s_1\, s_2\, dw_o \qquad (15)$$

The cylinder increments are easily written up as:

$$\frac{d}{da}(F_{cyl.} - U_{cyl.}) = \frac{t\, \sigma_{hoop}^2\, \pi\, a}{E} = \frac{p^2 \rho^2\, \pi\, a}{E\, t} \qquad (16)$$

Substitution of Eqs.(15) and (16) into Eq.(12) leads to :

$$G = \frac{p^2\, \rho^2\, \pi\, a}{E\, t} + \frac{1}{3} p\, s_1\, s_2\, \frac{dw_o}{da} \qquad (17)$$

Without bulging the last term should be dropped. The bulge factor can thus be expressed as :

$$\beta_b = \frac{K_{curved}}{K_{flat}} = \sqrt{\frac{G_{with\ bulging}}{G_{without\ bulging}}} = \sqrt{1 + \frac{E\, t\, s_1\, s_2\, dw_o/da}{3\, \pi\, a\, \rho^2\, p}} \qquad (18)$$

In other words, β_b can be obtained as a function of the characteristics of the deformation field of the bulged area (s_1, s_2 and dw_o/da). The measurements of the bulge deformation indicate that the values of s_1 and s_2 are approximately constant for different internal pressures p and equal to about 2 and 2.5 times the semi-crack length a respectively (see e.g. Fig.10). An evaluation of the $w_o(a,p)$ results suggests that dw_o/da can be approximated by:

$$\frac{dw_o}{da} = 0.316 \tanh\left(0.06\frac{\rho}{t}\sqrt{\frac{pa}{Et}}\right) \qquad (19)$$

Substitution of $s_1 = 2a$, $s_2 = 2.5a$ and the last equation in Eq.(18) gives:

$$\beta_{b,uniaxial} = \sqrt{1 + \frac{5}{3\pi}\frac{Eta}{\rho^2 p}0.316 \tanh\left(0.06\frac{\rho}{t}\sqrt{\frac{pa}{Et}}\right)} \qquad (20)$$

With this equation crack growth rates in pressurized (uniaxial) specimens can now be predicted. Figure 16 shows a rather good agreement ($\chi = 0$ results).

For biaxially tested specimens the crack growth rate was found to be systematically lower (Fig.9). As said before, the bulge deformation field could not be measured for this case. It should be expected that the ratios s_1/a and s_2/a will not be different, but da/dw_o with be significantly lower. Good predictions were obtained by dividing dw_o/da by $\sqrt{(1 + 18\chi)}$, which leads to:

$$\beta_b = \sqrt{1 + \frac{5}{3\pi}\frac{Eta}{\rho^2 p}\frac{0.316}{\sqrt{1 + 18\chi}}\tanh\left(0.06\frac{\rho}{t}\sqrt{\frac{pa}{Et}}\right)} \qquad (21)$$

A comparison of predicted crack growth rates obtained with this equation with test results again show a very good agreement, see Figures 12 and 16 ($\chi = 0.24$ results).

In summary, the bulge factor derived here is partly based on fracture mechanics considerations, and for another part on experimental observations of the bulge deformation field. The question to be considered now is whether the β_b equation has a wider applicability. If the conditions of a thin-walled cylinder are mainly defined by the internal pressure p, the biaxiality χ, and the dimensions ρ and t, the problem appears to have a similar character. It may then be expected that Eq.(21) can be used. This will be verified with results available in the literature.

APPLICATION OF THE BULGE FACTOR EQUATION TO RESULTS OF THE LITERATURE

Stress intensity factors for cracks in pressurized cylinders have been proposed in the literature. The factors are partly based on experiments and partly obtained from a fracture mechanics analysis. The experimental bulge factors were derived from bursting tests on unstiffened cylinders (6,7) and fatigue tests and analysis of DC-10 panels by Swift (8,9). A simple empirical equation was suggested:

$$\beta_b = 1 + C\frac{a}{\rho} \qquad (22)$$

where C = 9.2 according to Peters and Kuhn (6) and C = 10 according to Swift (9). It should be noted that the equation assumes a linear crack edge bulging effect, without a non-linear influence of the internal pressure p.

A linear behaviour was also assumed in several analytical approaches (10-18), noteworthy by Folias (10,11) and Erdogan and Kibler (12,13). However, finite-element calculations by Riks (19) and Ansell (20) indicated that a significant non-linear behaviour does occur. The bulge deformations are substantially smaller than according to the linear calculation, and due to the non-linear behaviour they are a function of the internal pressure p.

FEM calculation results of Riks (19,21) for unstiffened pressurized cylinders are shown in Figure 17. The agreement with the predictions according to Eq.(21) are quite good. Note the non-linear effect of the internal pressure on the bulge factor and the remarkable reduction of bulging at a higher pressure, see Fig.17b. A similar graph was obtained by Ansell (20).

FEM calculation results of Ansell are shown in Figure 18. The agreement is still reasonable, although it is not as good as in Fig.17. The discrepancies might be due to Ansell's calculation procedure of K_β in which the bulge bending contribution is ignored. Moreover, in our equations β_b for a very low p goes to infinity, which is obviously incorrect.

Swift (9) made an analysis for fuselages with frames and stiffeners. He paid special attention to the so-called 2-bay crack, see Figure 19. Swift suggests that the bulge effect has a maximum when the crack tips of a 2-bay crack are midway between the frames, where it is not affected by the central frame. It implies that β_b is equal to the bulge factor of an unstiffened cylinder. As a consequence, Eq.(21) should be applicable for that crack length. Swift further observed that the bulge effect is damping out when the crack tips approach the frames. He suggests that the damping out can be accounted for by introducing a cosine function, while considering the 2-bay crack as two separate cracks (length 2a) each starting from the frame. Swift proposes the cosine damping function to be*:

$$DF_{2\text{-bay-crack}} = \frac{1 - \cos(4\pi a/L)}{2} \qquad (23)$$

where L denotes the frame spacing. The damping factor must be applied to the maximum bulge factor in the bay, i.e. β_b for 2a = L/2. Substitution of this value in Eq.(21) and combining it with Eq.(23) leads to an equation for the bulge factor of a 2-bay crack with an intact frame:

* Swift wrote the numerator in Eq.(23) as $1 + \cos[\pi(1 - 4a/L)]$, which is the same.

$$\beta_{b,2\text{-bay-crack}} = \sqrt{1 + \frac{5}{12\pi}\frac{EtL}{\rho^2 p}\frac{0.316}{\sqrt{1+18\chi}}\tanh\left(0.06\frac{\rho}{t}\sqrt{\frac{pL}{4Et}}\right)\frac{1-\cos(4\pi a/L)}{2}} \qquad (24)$$

Based on Swift's considerations Mor (22) suggested the following bulge factor for a 1-bay crack:

$$DF_{1\text{-bay crack}} = \frac{1 + \cos(2\pi a/L)}{2} \qquad (25)$$

However, according to Mor, it should be applied to the bulge factor for the crack length a of the crack under consideration, which he substantiated by unspecified fatigue crack growth data. Substitution in Eq.(21) gives:

$$\beta_{b,1\text{-bay-crack}} = \sqrt{1 + \frac{5}{3\pi}\frac{Eta}{\rho^2 p}\frac{0.316}{\sqrt{1+18\chi}}\tanh\left(0.06\frac{\rho}{t}\sqrt{\frac{pa}{Et}}\right)\frac{1+\cos(2\pi a/L)}{2}} \qquad (26)$$

Swift's observations were made on DC-10 test panels with a relatively large longeron spacing S. Because the bulge phenomenon is dominated by the local out-of-plane deformation, longerons will certainly influence bulging if the longeron spacing is small as compared to the crack length. Unfortunately, simple arguments are not available for the question how to introduce the longeron spacing effect into Eqs.(24) and (26). Moreover, these equations have already an empirical character. The equations will still be checked with literature data for calculations on stiffened pressurized cylinders and full-scale fatigue tests on aircraft fuselages. It should be realized that in the present approach K_{flat} is simply equal to $\sigma_{hoop}\sqrt{\pi a}$ with $\sigma_{hoop} = p\rho/t$.

Calculated results were presented by Lemaître et al. (23), Riks (19) and Ansell (20). The results of Lemaître et al. for a 1-bay crack midway between the frames are presented in Figure 20. In the calculations it was assumed that radial displacements of the skin are zero at the locations of the frames and the longerons. In Figures 20a, b and d the longeron spacing is 200 mm and the results do agree fairly well with the predictions according to Eq.(26). A significant effect of the radius (ρ) is observed in Figure 20a, i.e. bulging is more significant for smaller aircraft. Figure 20c shows the influence of the longeron spacing. The bulge factor is significantly lower for the smallest spacing (S = 100 mm). This trend is not covered by Eq.(26). It anyhow should be expected that a small longeron spacing will lead to a considerable restraint on bulging deformations. Figure 20d again shows the reduction of β_b for a larger differential pressure.

Lemaître et al. also calculated β_b for another fuselage configuration with a 1-bay crack and ρ = 835 mm, t = 0.8 mm, a = 75 mm, L = 430 mm, S = 200 mm, p = 0.35 bar and χ = 0.5. The FEM calculation gave β_b = 2.05 which is rather close to the Eq.(26) value of 1.93.

FEM results of Riks (19), also for a midbay crack, are shown in Figure 21. He allowed radial displacements of the frames and the longerons. The results for a longeron spacing of 150 and 300 mm show smaller β_b values for a narrower spacing. The agreement with the predictions of Eq.(26) is poor, and moreover the calculations showed an obvious asymmetric behaviour. It should be noted that Riks for simplifying the calculation introduced cracks in all fields between stringers and frames. That might explain part of the asymmetry of his calculation results.

Ansell (20) in his FEM calculations also allowed radial displacements of frames and longerons. His results are compiled in table 1. The general agreement is good.

R (mm)	t (mm)	2a (mm)	p (bar)	bulge factor (ßb)		ratio
				Ansell	Eq.(24)	
2000	1.0	125	1.0	1.21	1.24	1.02
		250		1.47	1.45	0.99
		375		1.45	1.24	0.86
		125	0.6	1.26	1.36	1.08
		250		1.55	1.63	1.05
		375		1.57	1.36	0.89
2000	1.6	250	1.0	1.51	1.50	0.97
1000	0.5			1.96	1.83	0.93
	0.8			1.91	2.02	1.06

Table 1 : FEM results of Ansell (20) compared to predictions. (2-bay crack, frame spacing L = 500 mm, longeron spacing S = 200 mm)

The empirical results of Swift on full-scale DC-10 panels did agree with Eq.(22):

$$\beta_b = 1 + 10\frac{a}{\rho} \qquad (27)$$

This equation is the most well known one in the aircraft industry. In Figure 22 the equation is compared to the prediction of Eq.(21) as applied to the DC-10 test conditions. It shows a very good agreement. However, it should be noted that Swift's equation does not contain the pressure p, which has a significant influence on the bulge factor, as shown by the work of Riks, Ansell and Lemaître et al., as well as our own test results. Also the effect of the biaxiality ratio χ is not accounted for. As a result, equation (27) can only be a reasonable approximation, provided that the conditions are similar to those of the DC-10.

Schwarmann (24) reported on fatigue crack growth of three cracks in a pressurized fuselage structure:

- Crack A: a 1-bay crack midway between two frames (spacing L = 508 mm)

and midway between two longerons (spacing S = 160 mm).
- Crack B: a 2-bay crack located under a frame, midway between two longerons.
- Crack C: located midway between two frames, below a longeron.

Empirical bulge factors were derived from Schwarmann's crack growth curves by adopting a relevant da/dN-ΔK curve from which the effective (i.e. K_{bulge}) is read at several da/dN values found in the full-scale test. The β_b results can then be calculated. In table 2 a comparison is made to predicted values for crack A (1-bay crack, Eq.26) and crack B (2-bay crack, Eq.24). The agreement is rather good. Similarly obtained bulge factors for crack C were practically equal to 1, which should be associated with the fact that the cracked skin below the longeron behaves like a flat sheet.

	a	da/dN	bulge factor (ßb)		
	(mm)	(mm/kc)	test	prediction	ratio
crack A	30	3.2	1.20	1.20	1.00
	35	5.0	1.24	1.24	1.00
	40	7.8	1.27	1.28	1.01
	45	12.8	1.33	1.32	0.99
	50	19.3	1.36	1.36	1.00
	55	28.2	1.39	1.40	1.01
	60	54.1	1.47	1.43	0.97
crack B left tip	15	0.65	1.11	1.05	0.95
	20	1.23	1.15	1.09	0.95
	25	1.90	1.16	1.14	0.98
	30	2.72	1.16	1.19	1.03
crack B right tip	15	0.47	1.01	1.05	1.04
	20	1.00	1.09	1.09	1.00
	25	2.66	1.20	1.14	0.95
	30	6.50	1.41	1.19	0.84

Table 2 : Full-scale test results of Schwarmann (24). Comparison of empirical and predicted bulge factors. Material 2024-T3 Alclad, t = 0.8 mm, R = 1435 mm, frame spacing L = 508 mm, longeron spacing S = 160 mm, p = 0.47 bar.

Barrois (14) reported on fatigue crack growth in a full-scale test on the SN601A (Corvette). The K_{bulge} was determined for p = 0.4 bar by measuring the crack opening displacement. Crack growth results were obtained at several p-values, but the measured K-values can only be used for p = 0.4 bar because K is not proportional to p due to the non-linear behaviour. Moreover the crack growth

rate showed a considerable scatter. The comparison is thus restricted to the measured K-values and predicted results according to Eqs.(24) and (26). The data are presented in table 3. The agreement is quite good.

p (bar)	L (mm)	a (mm)	ßb		ratio
			test	prediction	
1-bay crack, front fuselage section					
0.4	260	76.3	1.61	1.51	0.94
2-bay crack, rear fuselage section, left crack tip					
0.4	430	37.75	1.66	1.60	0.96
2-bay crack, rear fuselage section, right crack tip					
0.4	380	37.75	1.66	1.62	0.98
1-bay crack, rear fuselage section					
0.4	380	78.53	1.80	1.82	1.01

Table 3 : Full-scale test results of Barrois (14). Comparison of measured and predicted bulge factors. Material A-U4G1-T3 (≈ 2024-T3), t = 0.8 mm, ρ = 850 mm.

DISCUSSION

In the present investigation the phenomenon of crack edge bulging was clearly observed in pressurized sheet specimens under uniaxial loading. The effect on fatigue crack propagation was systematically unfavourable. It also turned out that crack edge bulging is a non-linear phenomenon. Further, a biaxial tension field reduced the bulging deformation. Starting from fracture mechanics principles a relation has been derived, which does account for the non-linear influence of the internal pressure and the biaxiality. However, simplifying assumptions had to be made in the derivation, while the empirically observed deformation field and biaxiality effect were introduced. As a result, the equations derived for the bulging factor $ß_b$ of a longitudinal crack in a pressurized cylinder can not be claimed to be analytically rigorous formula. In order to cover the effect of fuselage frames the equation for the unstiffened cylinder was modified by introducing two "damping" factors proposed in the literature. These damping factors also lack a rigorous background. The equations (24) and (26) were obviously obtained in a heuristic way. The fortunate conclusion is that the predictions obtained do generally agree rather well with available results from the literature on cracks in pressurized cylinders and fuselage structures, obtained in full-scale tests and FEM calculations. It implies that the well known equation of Swift has been extended in order to account for the non-linear effect of the internal pressure and for the biaxiality effect. The unfortunate conclusion is that the equations do not include the effect of the longerons. As long as the

longeron spacing is not small the longerons do not have a significant effect. However, the bulge effect is reduced by a small spacing, which is favourable from a practical point of view.

The alternative to simple calculations with Eqs.(24) and (26) is to carry out FEM calculations. In order to be sure that reliable results are obtained such calculations should be made by experienced stress analysts. The financial input required may be quite large. It then appears that the present equations can be most useful for first approximations, and depending on the results, they may even be sufficient.

In the present investigation some practical trends were observed. Apart from the favourable effect of the biaxiality, it was illustrated that crack edge bulging is more severe for smaller fuselages (see Fig.20). Further, the bulge factor is lower for a higher internal pressure. A fuselage designed for a higher differential pressure should have less crack edge bulging problems. Moreover, the thicker skin will give another small reduction of the bulge factor (Fig.20).

TESTS ON ARALL AND GLARE PANELS

ARALL and GLARE are fibre-aluminium laminates, developed in Delft, primarily for resistance against fatigue crack growth. The laminates are built up from very thin sheets of Al-alloys (e.g. 0.3 or 0.4 mm) and intermediate layers with high-strength aramid fibres (in ARALL) or advanced glass fibres (in GLARE). The unidirectional fibres are embedded in a thin metal adhesive layer (prepreg), and the laminated material is obtained in a normal autoclave bonding cycle. The crack growth resistance can be very high as a result of crack bridging. If a fatigue crack has been nucleated in the Al-alloy sheets, the fibres will bridge the crack and thus restrain crack opening. That effectively reduces the stress intensity at the crack tip. Crack growth slows down, and crack arrest may occur. The development and application of these new materials is described in (26,27). It appears that a large weight saving is possible for fatigue critical components, such as the wing tension skin and the fuselage skin.

Tests on ARALL and GLARE panels were carried out as part of the present investigation. The number of tests was limited because insufficient laminated material was available at that time. Fatigue crack growth tests were carried out flat SUPERBAT specimens and curved specimens in the CETS and PFSTS equipment.

The flat SUPERBAT specimens were made of ARALL 2H32, which consists of two 2024-T3 sheets (t = 0.3 mm) and a single prepreg layer of unidirectional aramid fibres (TWARON) in an epoxy adhesive (AF163-2), the total thickness being 0.82 mm. Two specimens were tested uniaxially and four specimens biaxially (χ = 0.28) at $\sigma_{1,max}$ = 120 MPa (R=0). The scatter was very low and

average curves are presented only, see Figure 23. It clearly shows the superiority of ARALL if compared to 2024-T3 for which uniaxial and biaxial loading give the same crack growth. Remarkably, for ARALL the biaxiality has a favourable effect. Along the fatigue cracks in ARALL some limited delamination in the fibre-adhesive layers occurs. The delaminated areas can easily be observed after the fatigue test when the Al-alloy layers are removed by chemically milling. It turned out that the delaminated area became smaller if the loading was biaxial. Two arguments can explain the biaxiality effect: (1) The lateral stress restrains out-of-plane bending of the delaminated Al-alloy crack edges and thus reduces the mode II driving force for delamination. (2) The biaxial stress promotes the so-called fibre-splitting mechanism, which implies cracks in the fibre layer parallel to the fibre direction. This mechanism is also favourable. It is described in detail in (27).

It should be pointed out that fibre failure behind the crack tip did occur in the tests. The fibre failure mechanism is associated with fibre pull-out (out of the cracks in the adhesive), which is not a fully reversible process. It is followed by fibre buckling, fibre damage and fibre failure after a number of cycles. It is observed especially if the minimum stress of the cyclic load is close to zero or negative. It does not occur if a positive minimum stress is applied and in post-stretched ARALL, because the fibres then remain under tension. It also does not occur in the glass fibres of GLARE, irrespective of the value of the minimum stress. The glass fibre behaviour is essentially different from the aramid fibre behaviour. The aramid fibre failure mechanism is extensively described in (27). In spite of the occurrence of fibre failure Figure 23 shows that ARALL is still significantly superior to 2024-T3.

ARALL specimens were also tested in the CETS equipment. In these tests the specimens were carrying a constant bending stress corresponding to the radius of curvature (ρ), and a cyclic tension stress again at a zero stress ratio (R=0). Two types of ARALL were tested, viz. 2H32 and 7H32. The composition of 2H32 was already given above. ARALL 7H32 is of the same composition, except that 7075-T6 sheets are used. The specimens were tested at σ_{max} = 150 MPa (R=0). The crack growth results are given in Figures 24a and 24b. A systematic curvature effect can be observed, the crack was growing slower for a smaller radius ρ. Again the delaminated areas were studied after chemical removal of the Al-layers. It revealed fairly complex pictures, but they could be understood by observations of the cross section of the specimen at the location of the crack. It indicated that more fibre failure occurred at the inner side (compression) of the curved specimen, where most fibres at the outer side (tension) remain intact, due to some tension stress at minimum load. Crack bridging is then maintained more effectively.

Some ARALL and GLARE panels were tested in the PFSTS equipment under a cyclic differential pressure of 0.56 bar, which for a pressure cabin corresponds to a flying altitude of about 10000 meters. The radius of curvature was 2000 mm and the test frequency was 0.25 Hz. The crack growth curves are presented in Figure 25. Since all test panels were tested at the same pressure level, the hoop stress is different for the panels in view of the different thicknesses. However,

the panels carry the same load per mm width of the specimen (= $\sigma_{hoop} \cdot t$ = the so-called running load), which allows a direct comparison.

The curves in Figure 25 show a slower crack growth for ARALL 2H32 as compared to 2024-T3, although it carries a much higher hoop stress, see the table in Fig.25. Moreover, at a longer crack length (a > 60 mm), where crack growth in 2024-T3 becomes unstable, the growth rate in the ARALL panel decreased. Some crack edge bulging could visually be observed on the ARALL panel, but it was much smaller than for the 2024-T3 panel. Because the fibres did not fail they restrain out-of-plane displacement. The GLARE panel and the thicker ARALL 2H33 panel show an extremely slow growth. The weight saving merits of the panels can be judged by comparing the $\gamma \cdot t$ (specific gravity times thickness), which is a direct measure for the panel weight. The last column of the table in Figure 25 indicates a weight saving of some 40% for the ARALL 2H32 panel if compared to the 2024-T3 panel with still a better fatigue crack growth resistance. For the GLARE panel the weight saving is 30% with a highly superior crack growth resistance.

Figure 25 also gives the crack growth curves for flat panels tested at approximately the same tensile stress. A detrimental effect of crack edge bulging can not be observed. As said before, the bulging was much less for the 2H32 panel, while for the other two panels the crack extension was too small to observe any bulging displacements.

CONCLUSIONS

Longitudinal cracks in a pressurized fuselage offer special problems, because the crack occurs in a *curved* thin sheet metal structure, and the conditions are complex due to the *biaxial loading* and the *internal pressure*. The fatigue crack edges bulge outwards (out-of-plane deformation), which considerably complicates the fracture mechanics analysis. The problem has been analyzed empirically and analytically. Three new test set-ups were designed for loading a sheet specimen biaxially (SUPERBAT specimen), for loading a sheet specimen in tension around a block with a fixed curvature (CETS equipment), and for loading a curved sheet specimen under hoop stress conditions by applying air pressure to the specimen (PFSTS equipment). The SUPERBAT specimen was also used in the latter test set-up. A realistic simulation of the pressurized fuselage condition is thus obtained. The main results are summarized in the following conclusions.

(1) The stress biaxiality (χ = 0.28) did not affect fatigue crack growth in both 2024-T3 and 7075-T6 flat sheet specimens.

(2) Specimens tested with the CETS equipment are subjected to constant bending stress and an applied tension load. The static tests revealed a systematic effect of the curvature on the residual strength for both 2024-T3 and 7075-T6. A smaller radius of curvature led to a lower residual strength. A analytical relation was developed for the residual tensile strength under this type of loading. Accurate predictions were obtained for the 7075-T6 sheet material, and surprisingly enough also for 2024-T3

specimens, although net section yielding occurred in this material.

(3) Fatigue tests (R = 0) with the CETS equipment showed the same crack growth rate for thin Al-alloy sheets ($t \leq 1$ mm) for curved and for flat specimens, provided the radius of curvature is sufficiently large. For small curvature radii (≤350 mm) the crack growth rate tends to decrease. This unexpected result is associated with a phenomenon *"partial crack closure due to bending"*, which is a result of the compressive stress at the compression side of the specimen. The phenomenon is different from the well known Elber's crack closure mechanism.

(4) Bulge out of crack edges is observed during the CETS experiments, especially if a small radius of curvature is applied. Bulge out can occur even without an internal air pressure.

(5) Tests in the PFSTS under air pressure indicate significant bulge out deformations. The deformation field has been measured. It turns out to depend in a non-linear way on the applied air pressure. Moreover, in comparison to uniaxial loading, the bulge out deformations are considerably smaller under biaxial loading. As a consequence the crack growth rate is smaller under biaxial loading.

(6) The experiments have shown that the bulge factor (β_b), defined as the ratio of the effective K-factor and the nominal K-factor (K_{bulge}/K_{flat}), decreases with increasing internal pressure and stress biaxiality, and increases with increasing crack length.

(7) FEM calculations made for pressurized aircraft skin structures (Riks, Ansell, Lemaître et al.) show that linear theories on bulge-out developed by Folias, Erdogan, etc. are invalid. The bulge out factor is a non-linear function of the loading conditions (Δp,biaxiality) and the geometrical parameters (ρ,t,a).

(8) Analytical relations for the bulge factor have been developed, based on an energy balance approach, and on empirical observations of the bulge-out deformation field. The analysis has led to equations for a non-linear bulge factor. Predictions with the equations agree rather well with the results of the present investigation and with FEM results and full-scale test results from the literature. The effect of fuselage frames can be accounted for by adopting a damping factor presented in the literature. However, the theory is unable to predict the effect of the longeron spacing on the bulge-out factor. Fortunately, stiffening elements decrease bulge out.

(9) The well known bulge formula of Swift gives good predictions for fuselage structures similar to the DC-10 configuration (i.e. $p \approx 0.57$ bar, $\rho/t = 1500$ and a stress biaxiality ratio of 0.5). However, for other configurations Swift's formula gives erroneous bulge factors.

(10) Test results show that stress biaxiality leads to a lower crack growth rate in ARALL laminates. There are two reasons: a biaxial stress field restrains the out-of-plane deformation, which leads to a smaller delamination area, and secondly, stress biaxiality enhances fibre splitting in the delamination area. Both mechanisms lead to a lower crack growth rate.

(11) "Partial fibre failure" in the aramid prepreg was observed in the CETS fatigue tests (R = 0) on ARALL specimens. The aramid fibres on the tension side of the specimen tend to remain intact more than on the

compression side, which leads to a lower crack growth rate. A higher bending stress (i.e. a smaller radius of curvature) did result in a lower crack growth rate.

(12) In contrast to monolithic aluminium sheets, bulge-out displacements in cracked ARALL are much smaller and have no influence on fatigue crack growth. Very low crack growth rates were obtained in curved specimens of ARALL and GLARE loaded by cyclic air pressure. If fatigue crack growth resistance is a predominant design criterion, large weight savings are possible.

NOTATIONS

L = frame spacing
Δp = range of pressure p
R = stress ratio
S = longeron spacing
t = sheet thickness
w = out-of-plane displacement
w_o, s_1, s_2 see Fig.15

β_b = bulge factor (K_{bulge}/K_{flat})
γ = density
ρ = radius of curvature
χ = biaxiality ratio (σ_2/σ_1)
1 bar = 14.5 psi

ACKNOWLEDGEMENT

The cooperation of several members of the Structures & Materials Laboratory (Faculty of Aerospace Engineering, Delft University of Technology) and instructive discussions with Dr.E.Riks of the National Aerospace Laboratory (NLR) have been much appreciated.

REFERENCES

(1) Chen,D., "Bulging of fatigue cracks in a pressurized aircraft fuselage". Doctor Thesis, Delft Un. of Tech., Report LR-647, Fac. of Aerospace Eng., Delft, 1991.

(2) Swift,T., "The effects of stress level, geometry, and material on fatigue damage tolerance of pressurized fuselage structure". Proc.14th ICAF Symp. on "New Materials and Fatigue Resistant Aircraft Design". Ed. by D.L.Simpson, EMAS, Warley, England, 1987, pp.1-77.

(3) Jong,G.J.de,"A solution for the problem of load introduction in biaxial fatigue tests". Nat. Aerospace Lab. NLR, Amsterdam, Report NLR-TP-90112, 1990.

(4) Miller,K.J. and Brown,M.W. (editors), "Multiaxial Fatigue", ASTM STP 853, Am.Soc.Testing Materials, 1985.

(5) McClung,R.C.,Fatigue Fract.Eng.Mat.Struct.,Vol.12,1989,pp.447-460.

(6) Peters,R.W. and Kuhn,P.,"Bursting strength of unstiffened pressure cylinders with slits". NACA Tech.Note 3993, 1957.

(7) Anderson,R.B. and Sullivan,T.L.,"Fracture mechanics of through-cracked

cylindrical vessels". NASA TN D-3252, 1966.
(8) Swift,T.,"The application of fracture mechanics in the development of DC-10 fuselage". AGARD-AG-176, 1974, pp.227-287.
(9) Swift,T.,"Design of redundant structures". AGARD-LS-97, 1979, pp.9-1 to 9-23.
(10) Folias,E.S.,"An axial crack in a pressurized cylindrical shell". Int. J. Fracture Mech., Vol.1, 1965, pp.104-113.
(11) Folias,E.S.,"Plates and shells", Mechanics of Fracture, Vol.3, Noordhoff Int. Publishing, 1979, pp.117-160.
(12) Erdogan,F.,"Plates and shells", Mechanics of Fracture, Vol.3, Noordhoff Int. Publishing, 1977, pp.161-200.
(13) Erdogan,F. and Kibler,J.J.,"Cylindrical and spherical shells with crack". Int. J. Fracture Mech., Vol.5, 1969, pp.229-237.
(14) Barrois,W., Eng.Fracture Mech., Vol.7, 1975, pp.673-688.
(15) Hahn,G.T., Sarrate,M. and Rosenfield,A.R., Int. J. Fracture Mech., Vol.5, 1969, pp.187-210.
(16) Copley,L.G. and Sanders Jr J.L., Int. J. Fracture Mech., Vol.5, 1969, pp.287-297.
(17) Murthy,M.V.V., Rao,K.P. and Rao,A.P., Int. J. Fracture Mech., Vol.8, 1972, pp.287-297.
(18) Ehlers,R., Eng. Fracture Mech., Vol.25, 1986, pp.63-77.
(19) Riks,E.,"Bulging cracks in pressurized fuselages: A numerical study". Nat. Aerospace Lab. NLR, Amsterdam, Report MP-87058, 1987.
(20) Ansell,H.,"Bulging of cracked pressurized aircraft structure". Inst. of Tech., Dept. Mech. Eng., Report LIU-TEK-LIC-1988:11, 1988.
(21) Riks,E. and den Reijer,P.J.,"A finite element analysis of cracks in a thin walled cylinder under internal pressure". Nat. Aerospace Lab. NLR, Amsterdam, Report TR-87021, 1987.
(22) Mor,H.,"Crack propagation analysis of longitudinal skin cracks in a pressurized cabin". 26th Israel Annual Conf. on Aviation and Astronautics, Tel Aviv., 1984, pp.78-83.
(23) Lemaître,J., Turbat,A. and Loubet,R., Eng. Fracture Mech., Vol.9, 1977, pp.443-460.
(24) Schwarmann,L.,"Crack propagation analysis of pressurized fuselage structure". AGARD-AG-257, 1980, pp.3-93.
(25) Gunnink,J.W., Vogelesang,L.B. and Schijve,J.,"Application of a new hybrid material (ARALL) in aircraft structures". Proc. 13th I.C.A.S. Congress, August 1982.
(26) Gunnink,J.W.and Vogelesang,L.B.,"Metal Laminates - The Advancements in Aircraft Materials". Conf. on Advanced Materials, 35th Int. SAMPE Symposium, Anaheim, California, 2-5 April 1990.
(27) Roebroeks,G.H.J.J. (1991), doctor thesis, to be published.

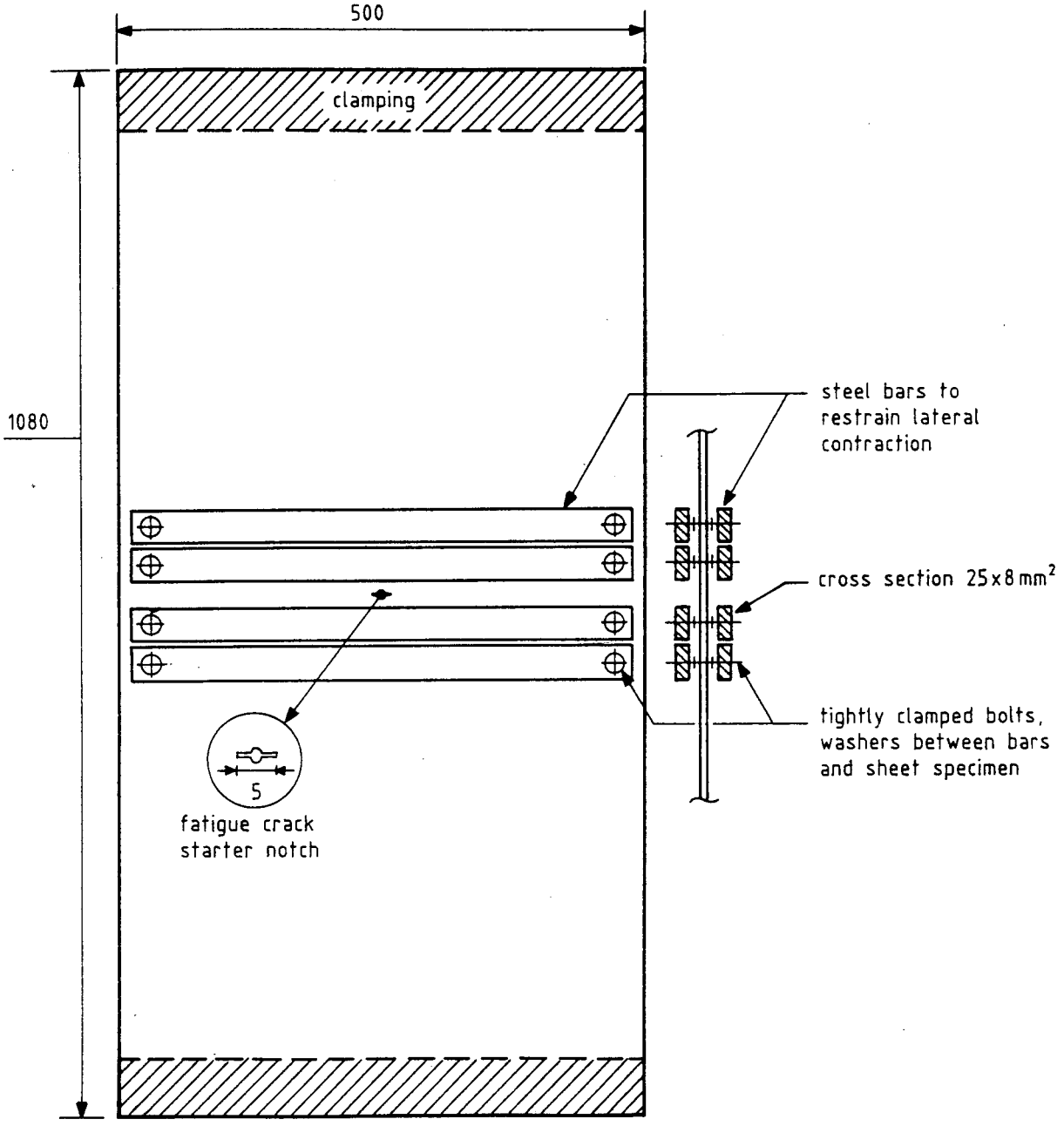

Figure 1: SUPERBAT specimen used for biaxial testing.

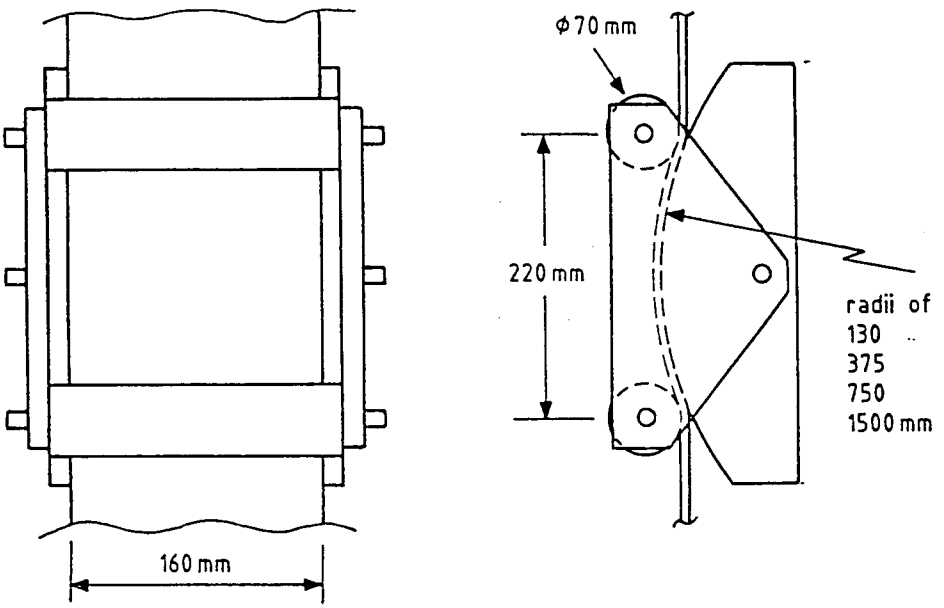

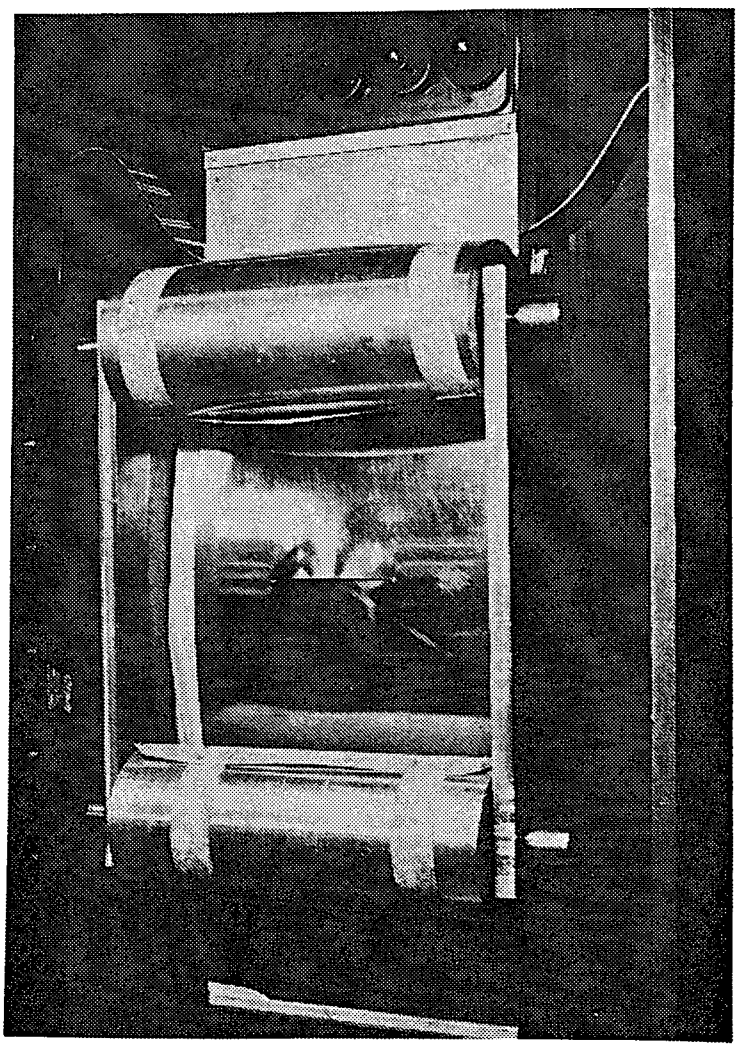

Figure 2 : CETS (Curvature Effect Test System)

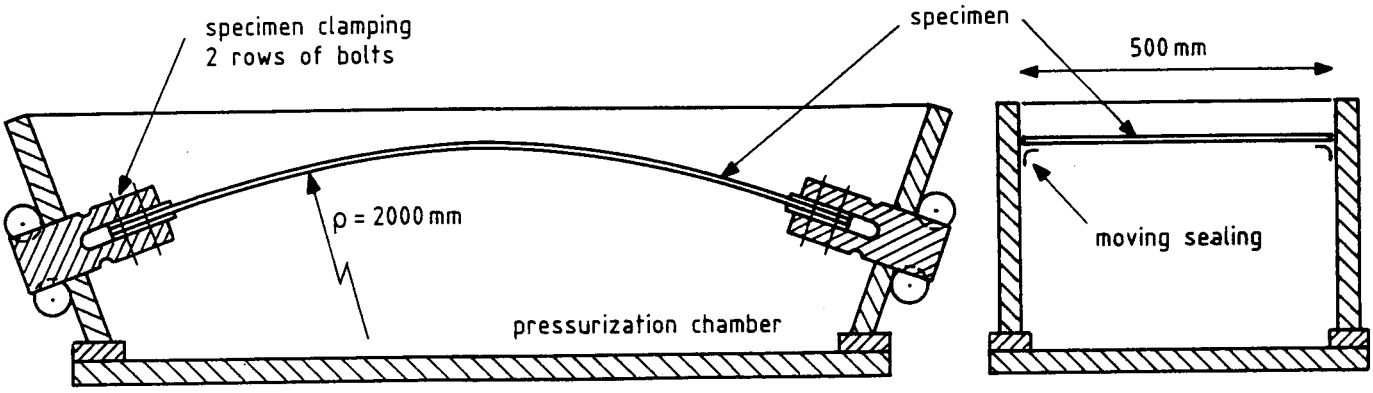

Figure 3 : Pressurized Fuselage Skin Test System (PFSTS).

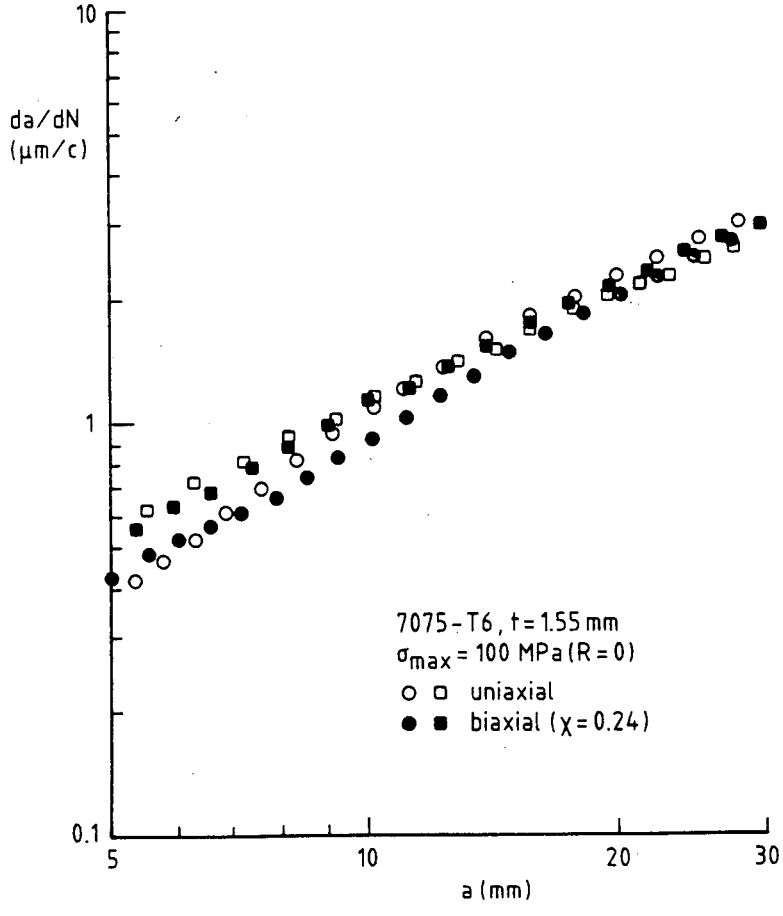

Figure 4 : Effect of biaxiality on the fatigue crack growth rate.

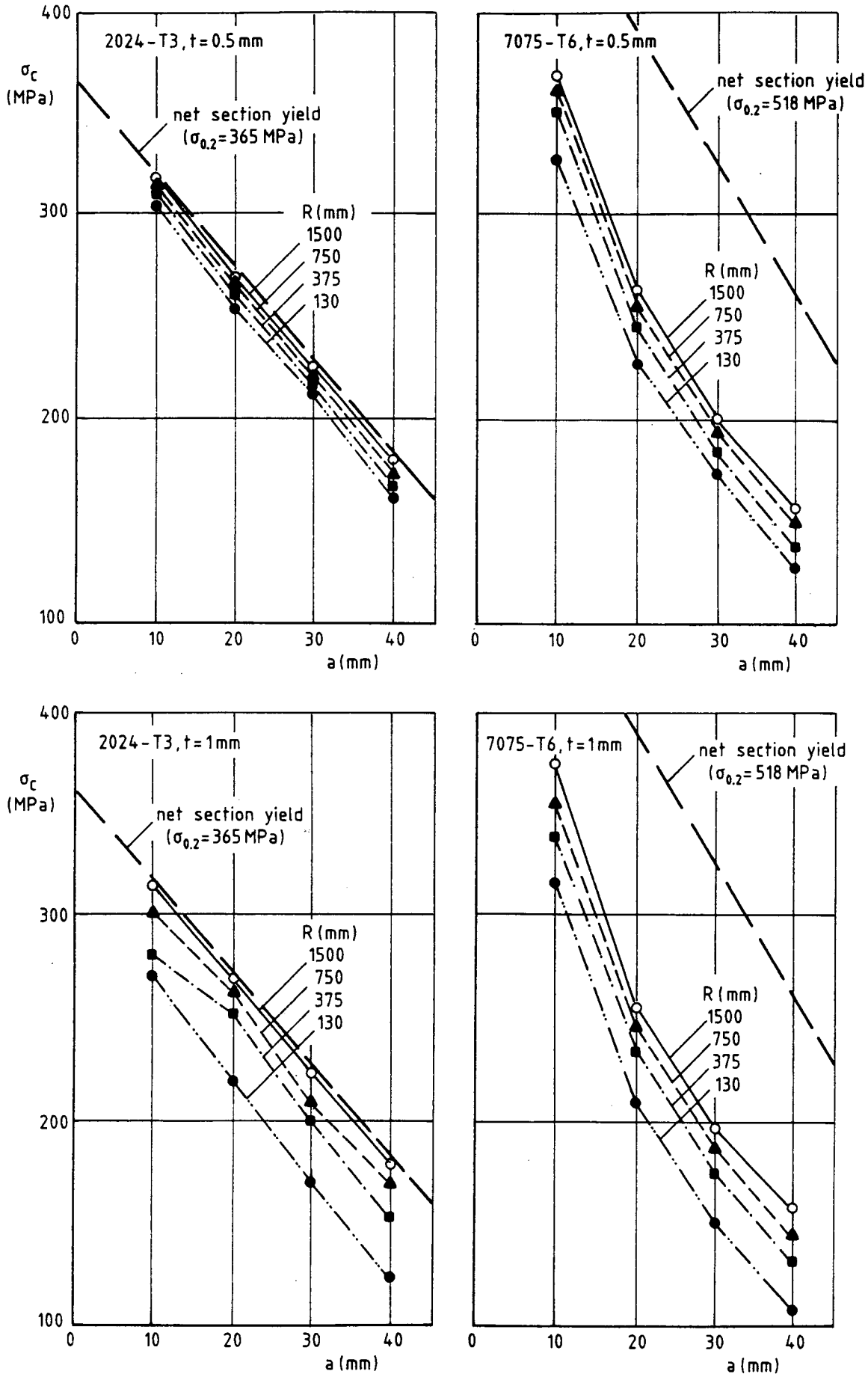

Figure 5 : Effect of curvature on residual strength (CETS results).

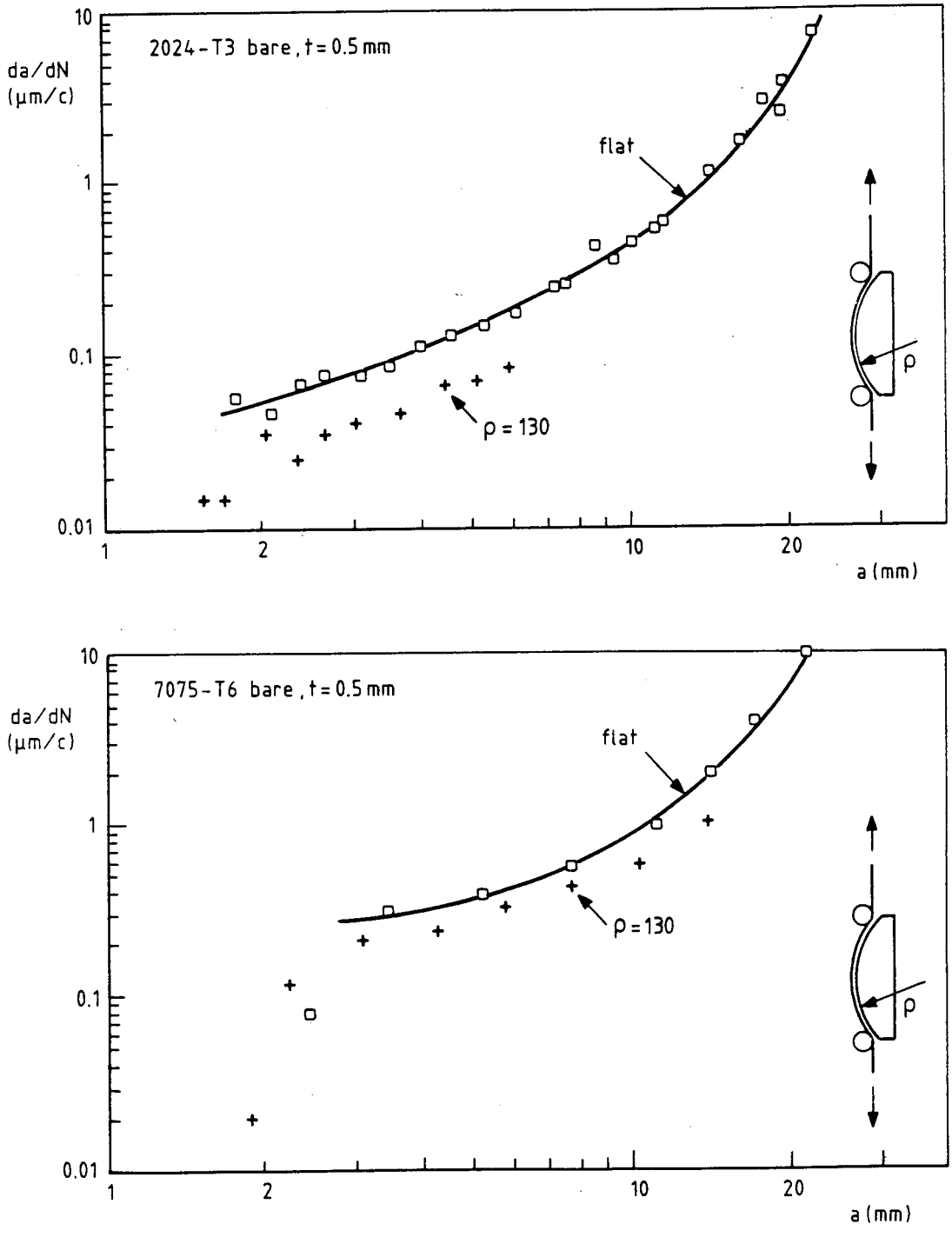

Figure 6 : Effect of curvature on fatigue crack growth (CETS results)

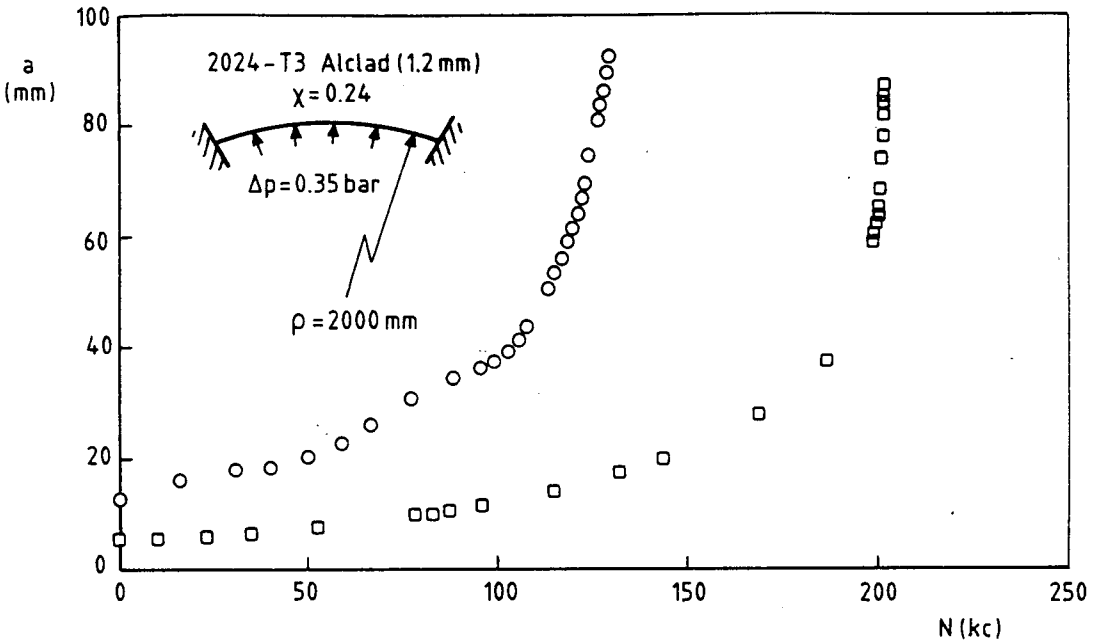

Figure 7 : Examples of crack growth curves obtained under internal pressure (PFSTS results).

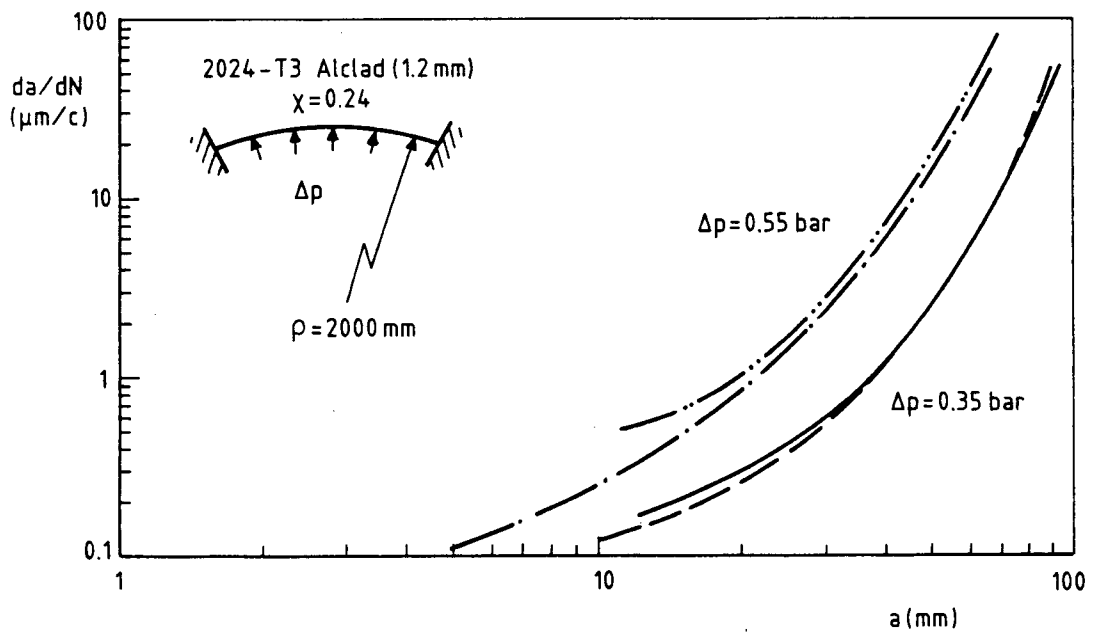

Figure 8 : Examples of crack growth rates under internal pressure.

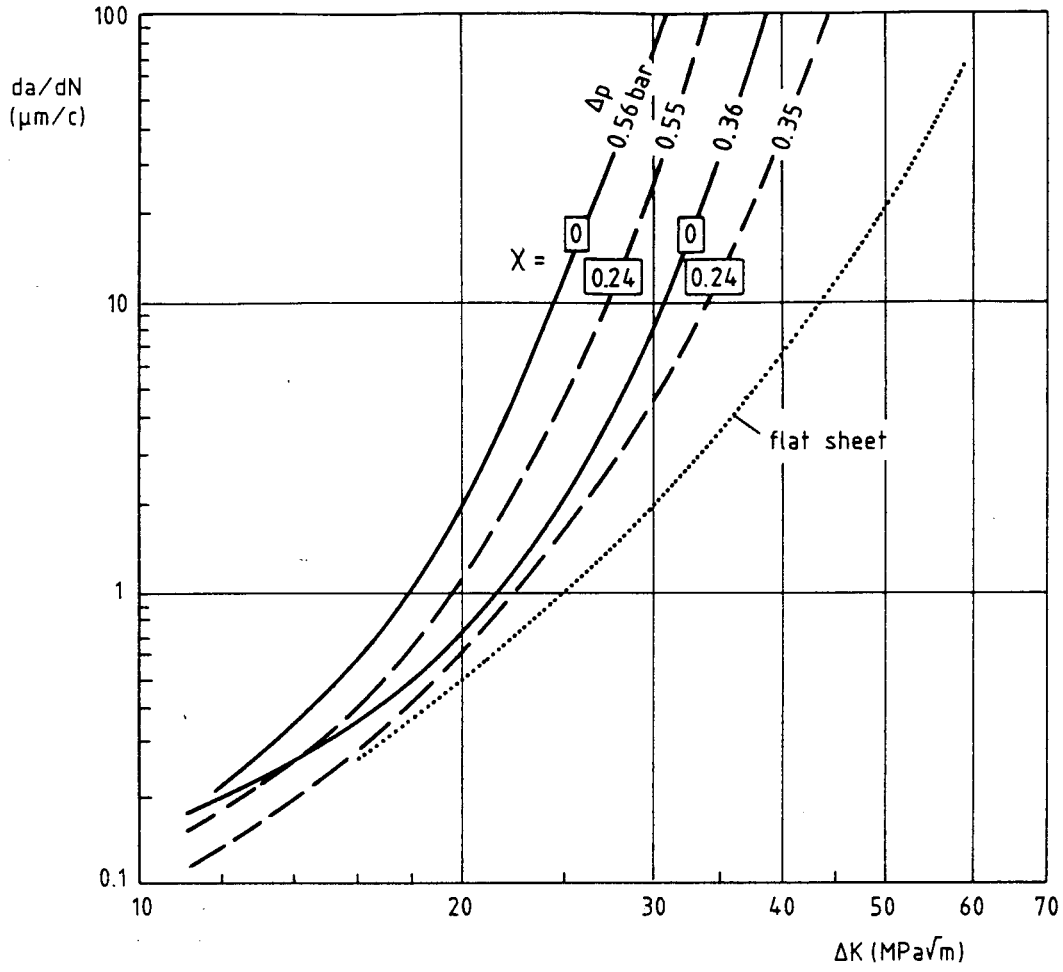

Figure 9 : Comparison of crack growth rates under cyclic air pressure.
Effect of pressure level and biaxiality.

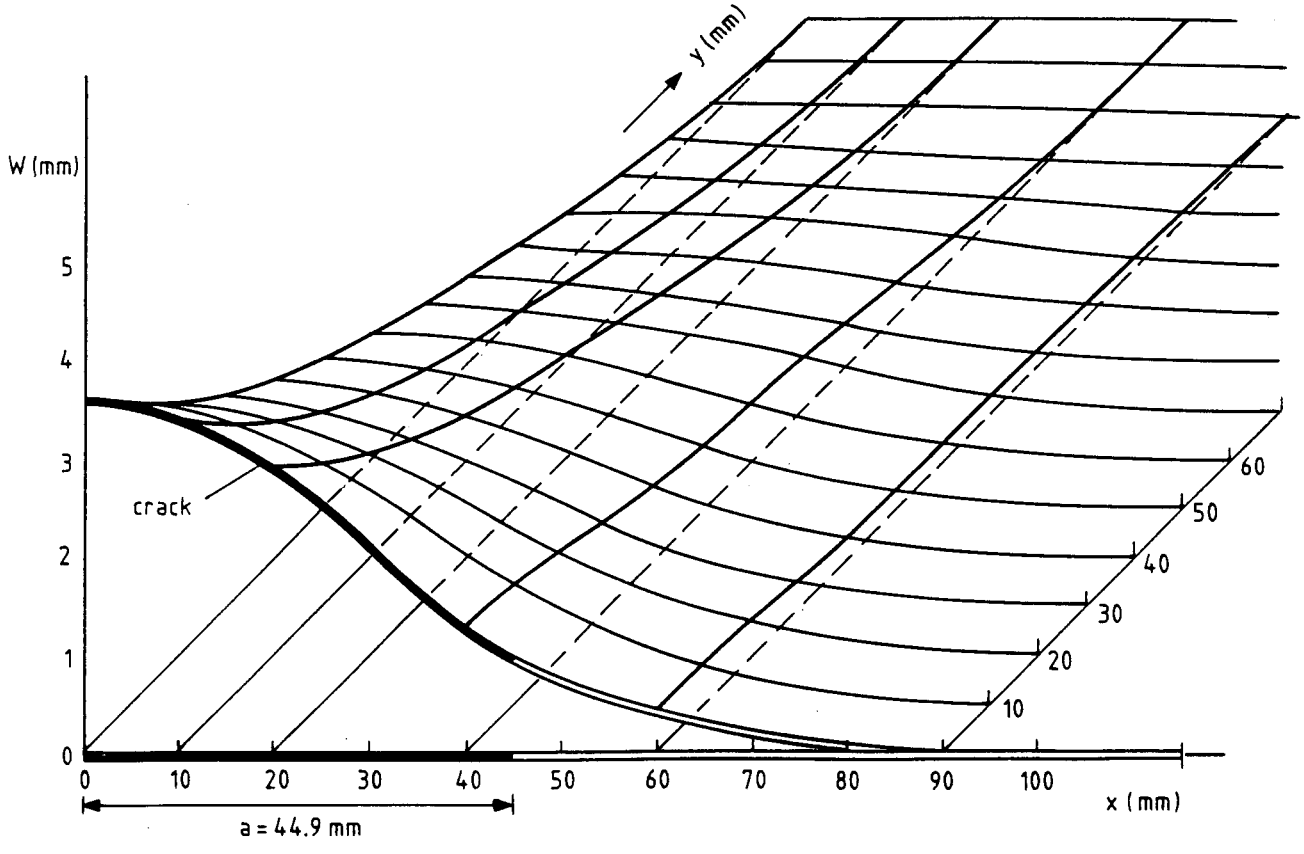

Figure 10 : Out-of-plane deformation field around a crack of 44.9 mm at Δp=0.55 bar.

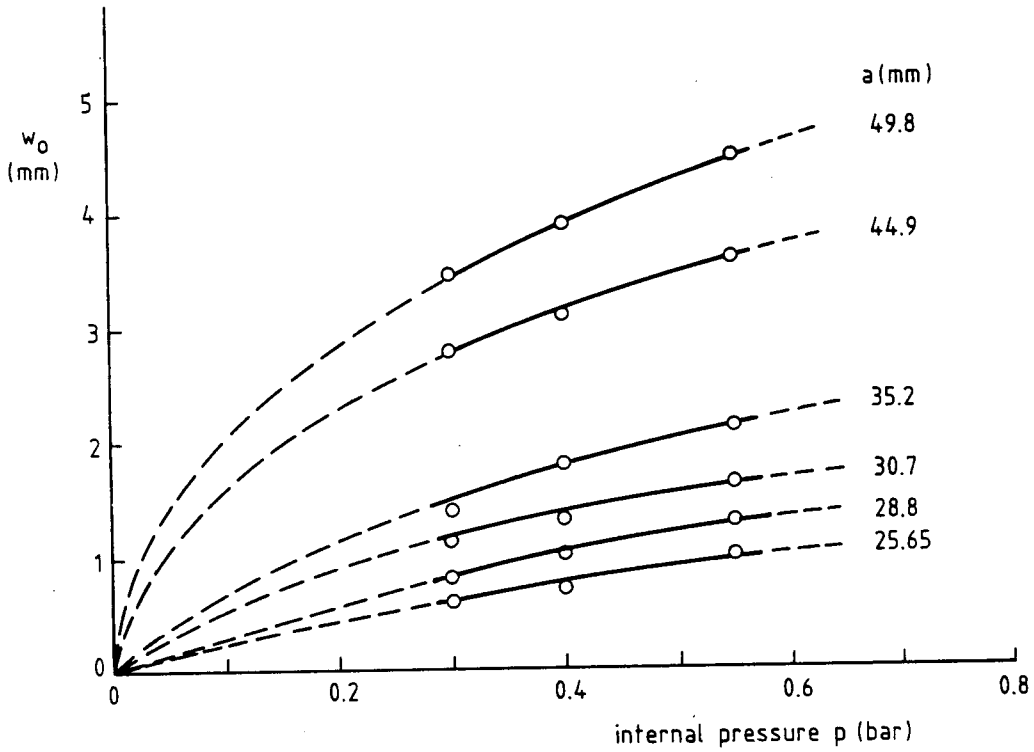

Figure 11 : Out-of-plane deformation of the center of the crack (w_o) as a function of internal pressure p.

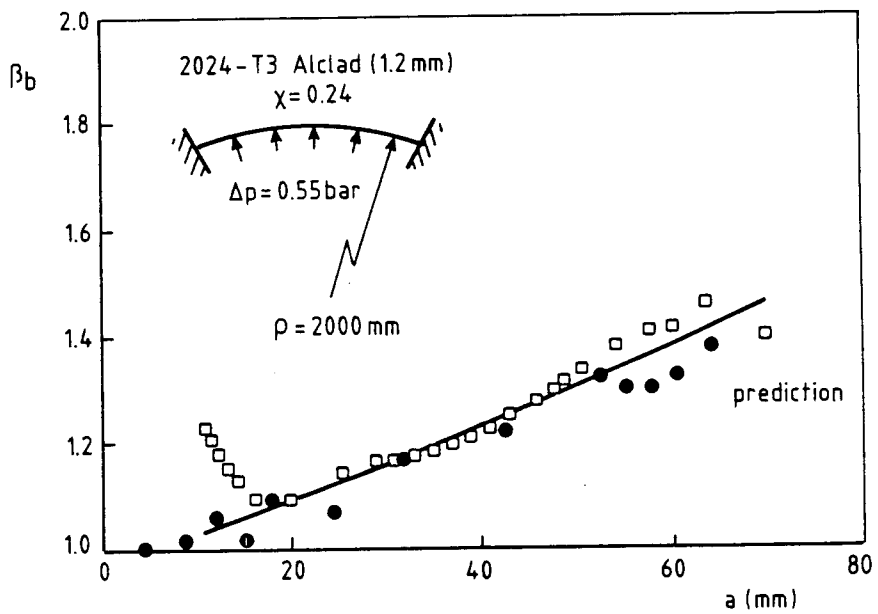

Figure 12 : The empirical bulge factor obtained in two similar tests.

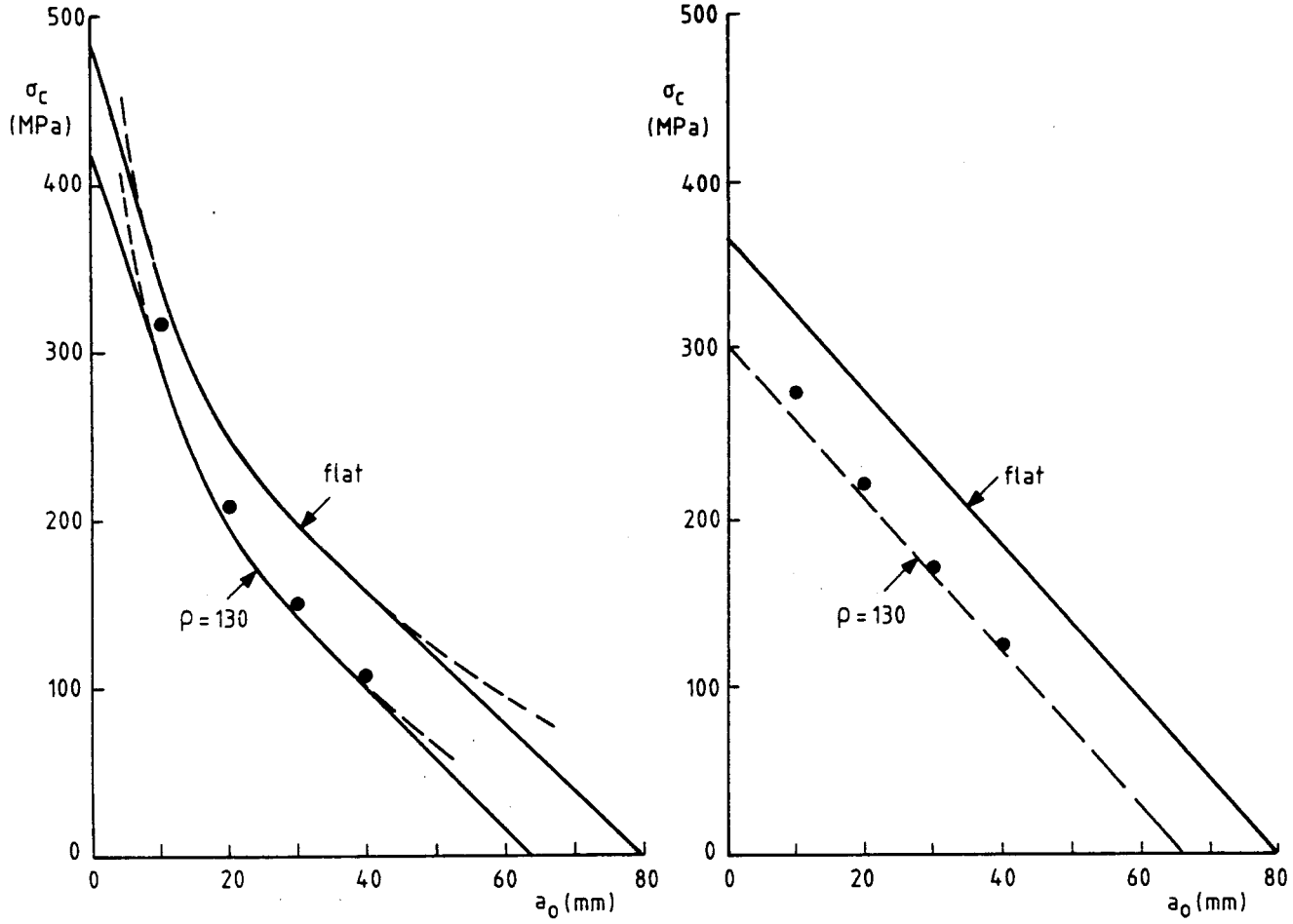

Figure 13 : Predicted Feddersen diagrams for strongly curved sheet.
Comparison with test results.

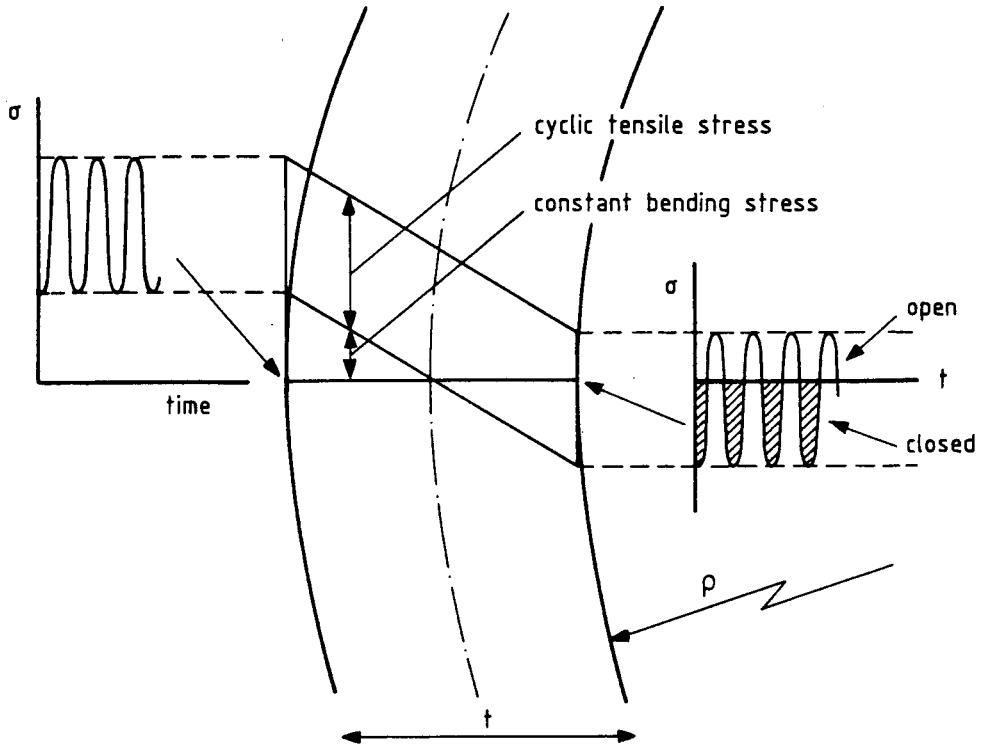

Figure 14 : Partial crack closure due to constant bending.

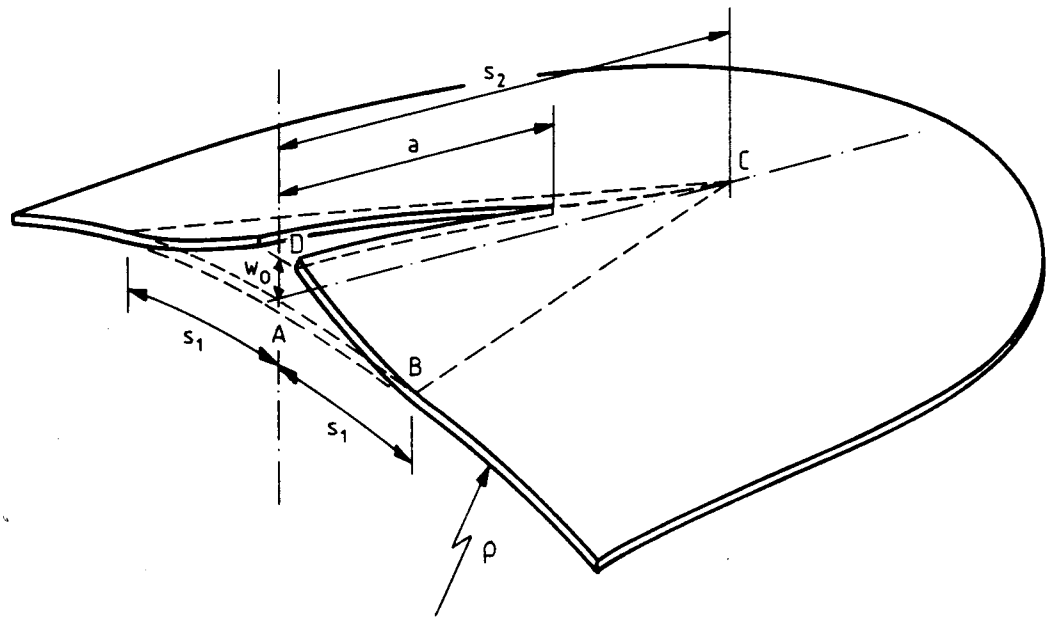

Figure 15 : One half of the bulged area.

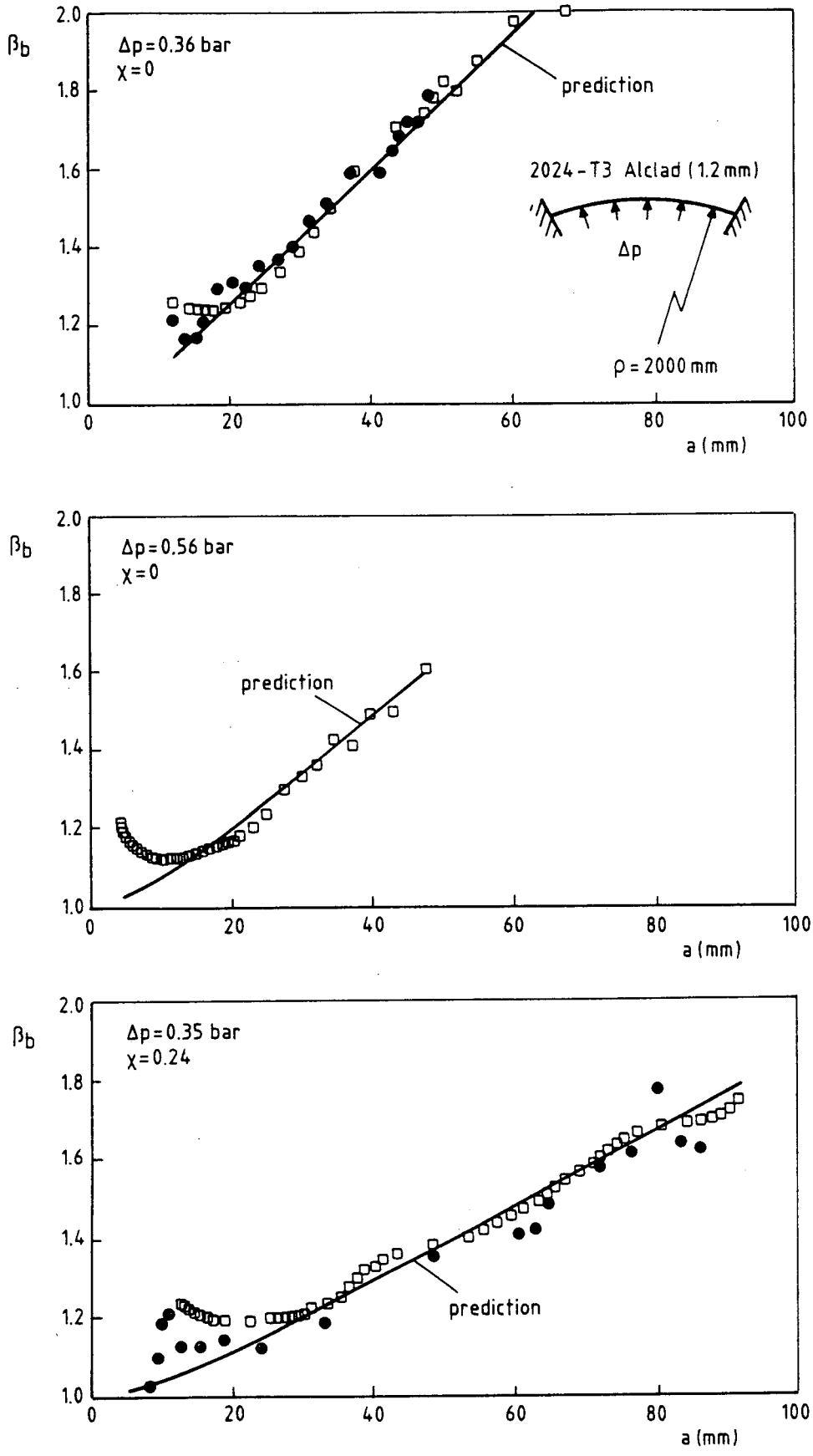

Figure 16 : Empirical bulge factors (see also Fig. 12) derived from pressurized panel tests (PFSTS). Comparison to predictions [Eq. 21].

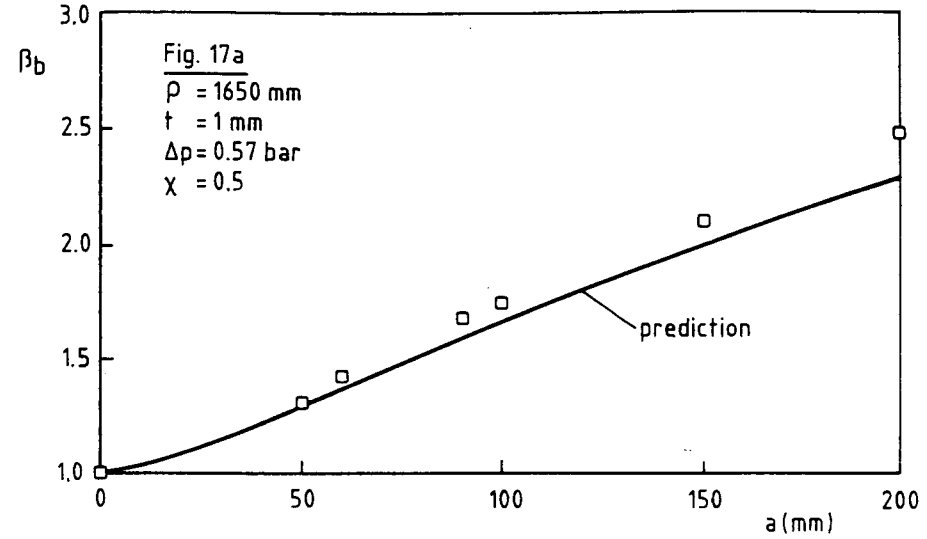

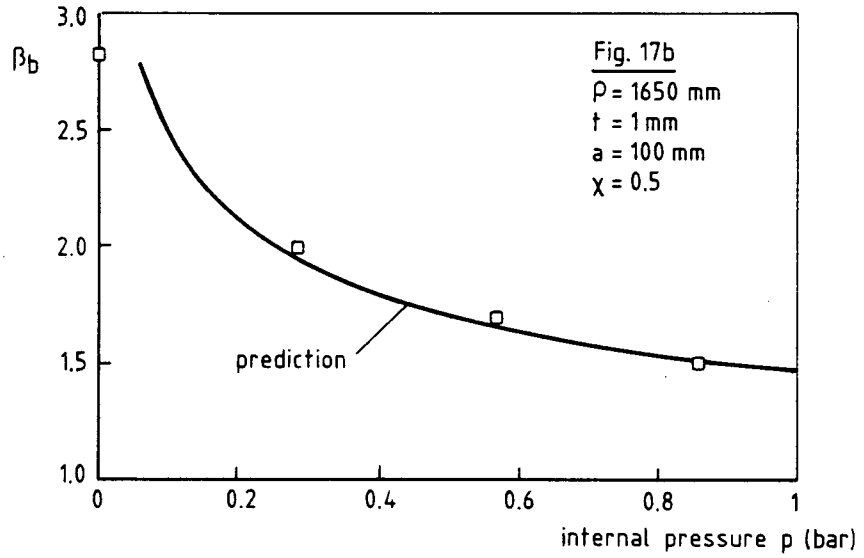

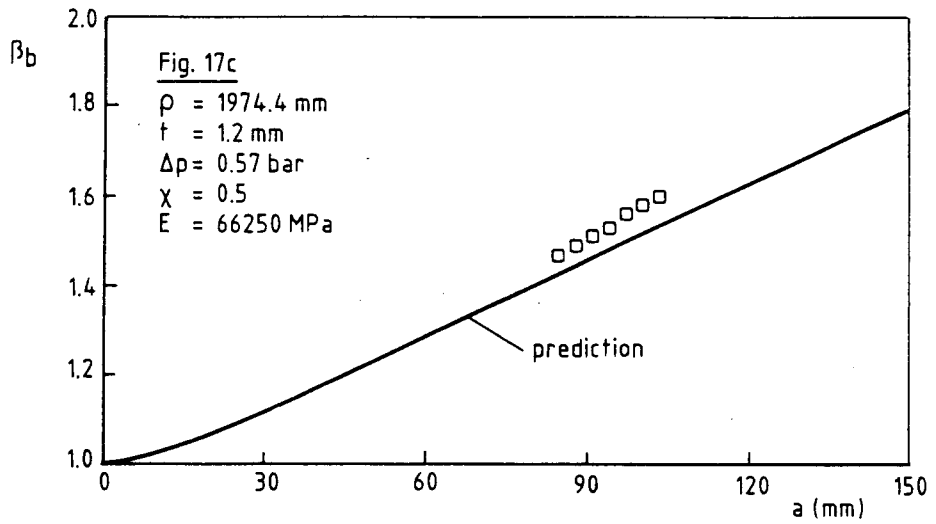

Figure 17 : FEM results of Riks et al [19,21]. Comparison to predicted bulge factors [Eq. 21].

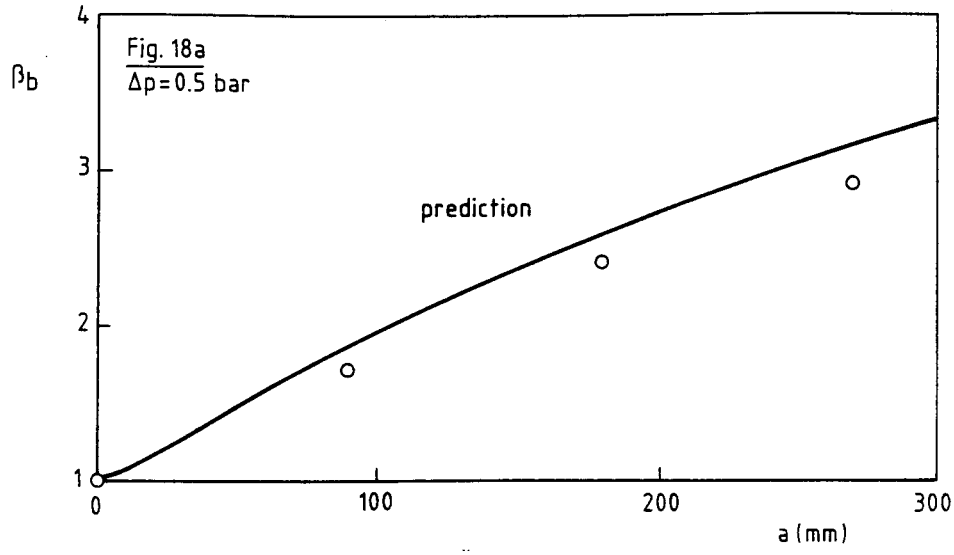

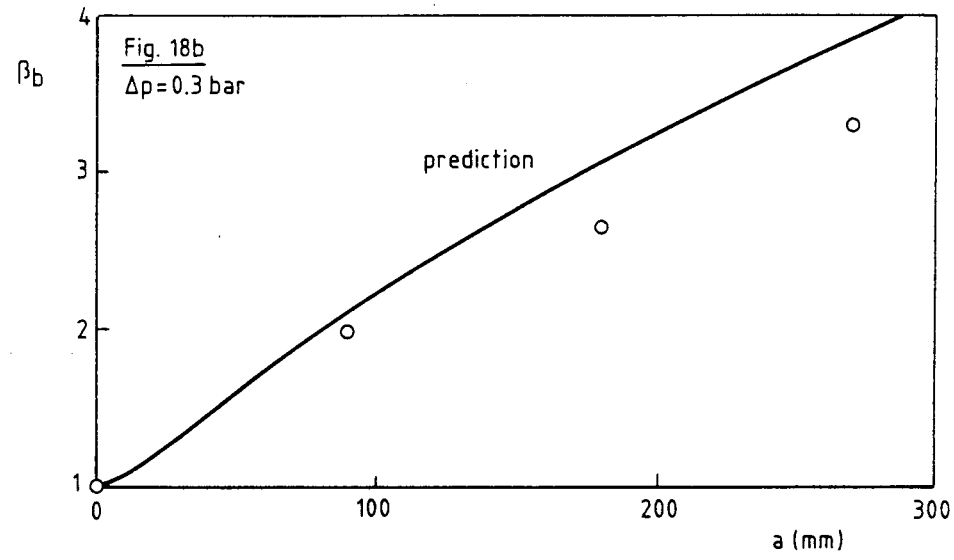

Figure 18 : Comparison of bulge factors calculated by Ansell (FEM results) [20] with prediction of Eq. [21]. Unstiffened cylinder, ρ = 1155.7 mm, t = 0.635 mm, χ = 0.5, Al-alloy.

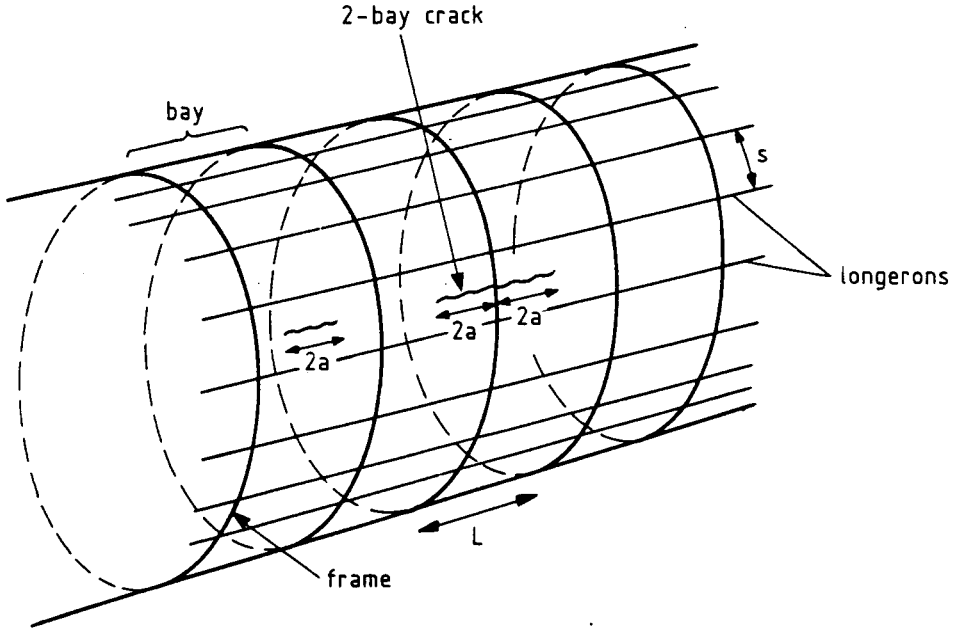

Fig. 19 : One-bay and two-bay crack.

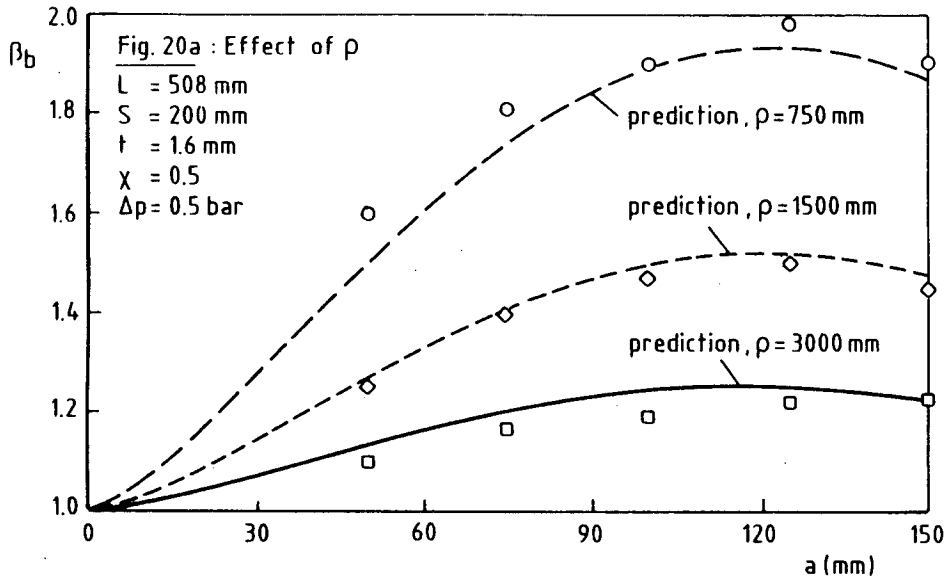

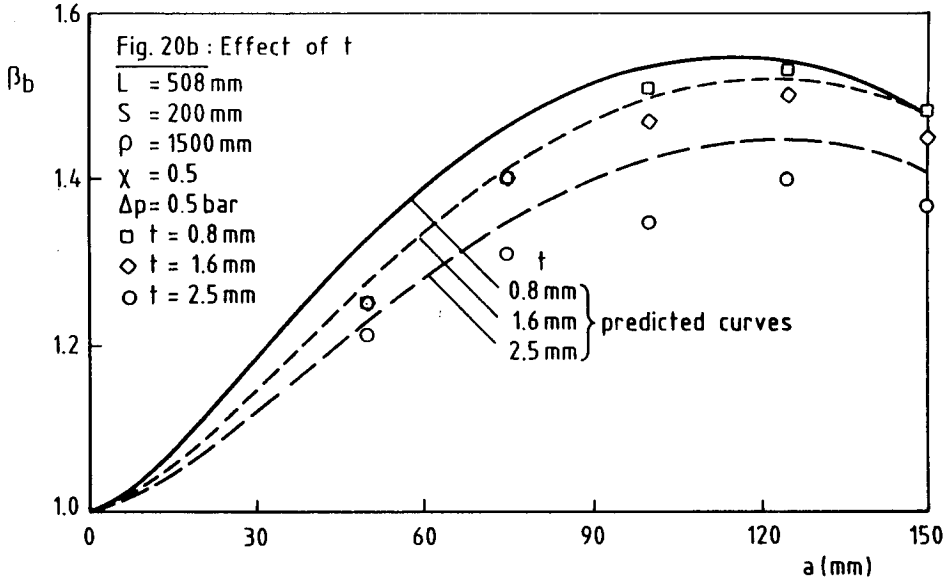

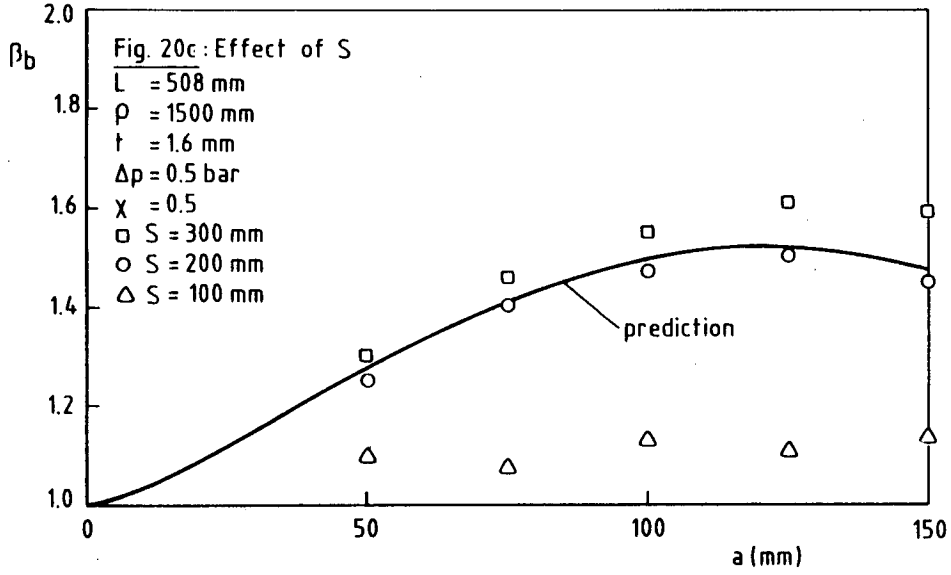

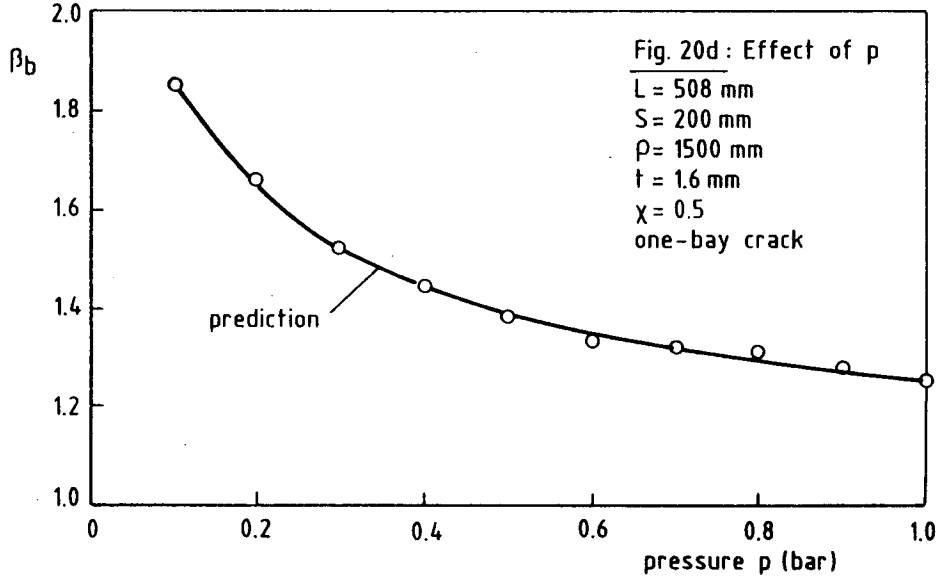

Figure 20 : Results of FEM calculations of Lemaître et al. [23] on the bulge factor of a one-bay crack in a pressurized fuselage structure. Comparison to predictions [Eq. 26]. L = frame spacing, S = longeron spacing.

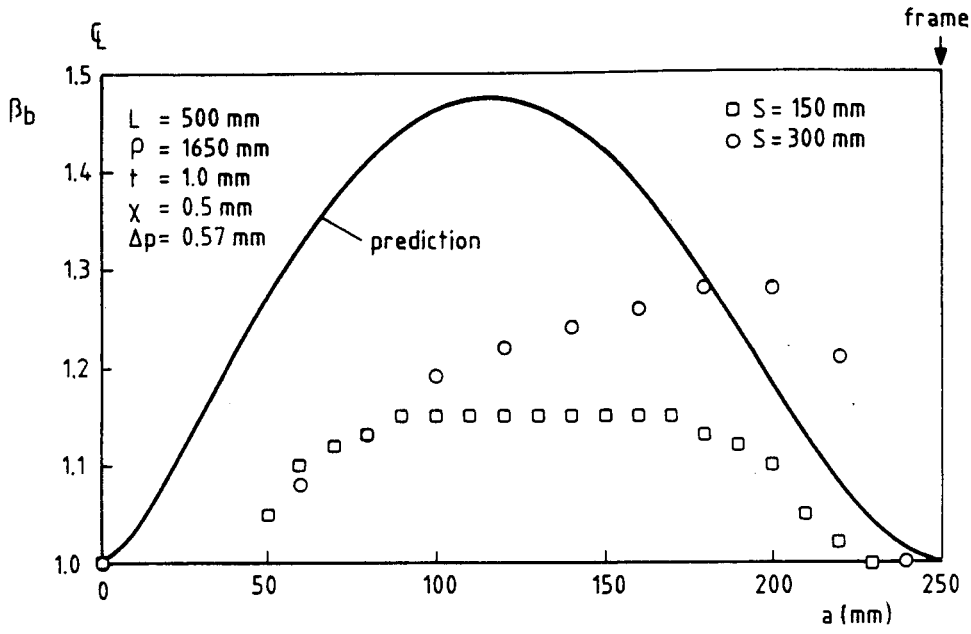

Figure 21: Results of FEM calculations of Riks [19] on the bulge factor of a one-bay crack in a pressurized fuselage structure. Comparison to predictions (Eq. 26).

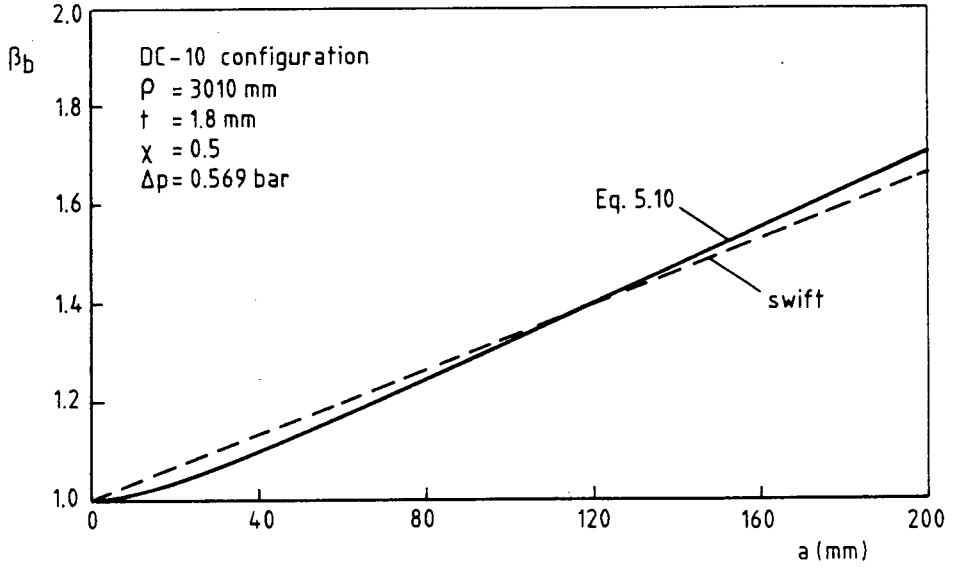

Figure 22: Comparison of Swift's equation with Eq. [21] for conditions (ρ, t, p, χ) applicable to the DC-10.

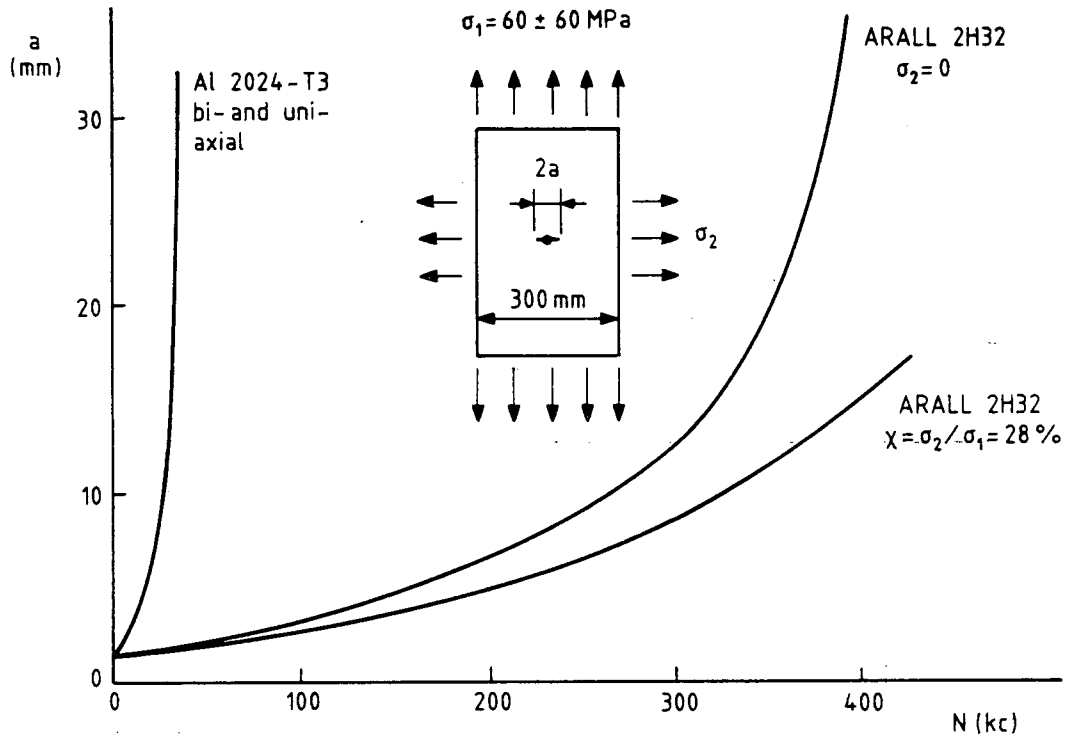

Figure 23 : Fatigue crack growth results of flat ARALL specimens (t=0.82 mm)
Effect of biaxiality and comparison to 2024-T3.

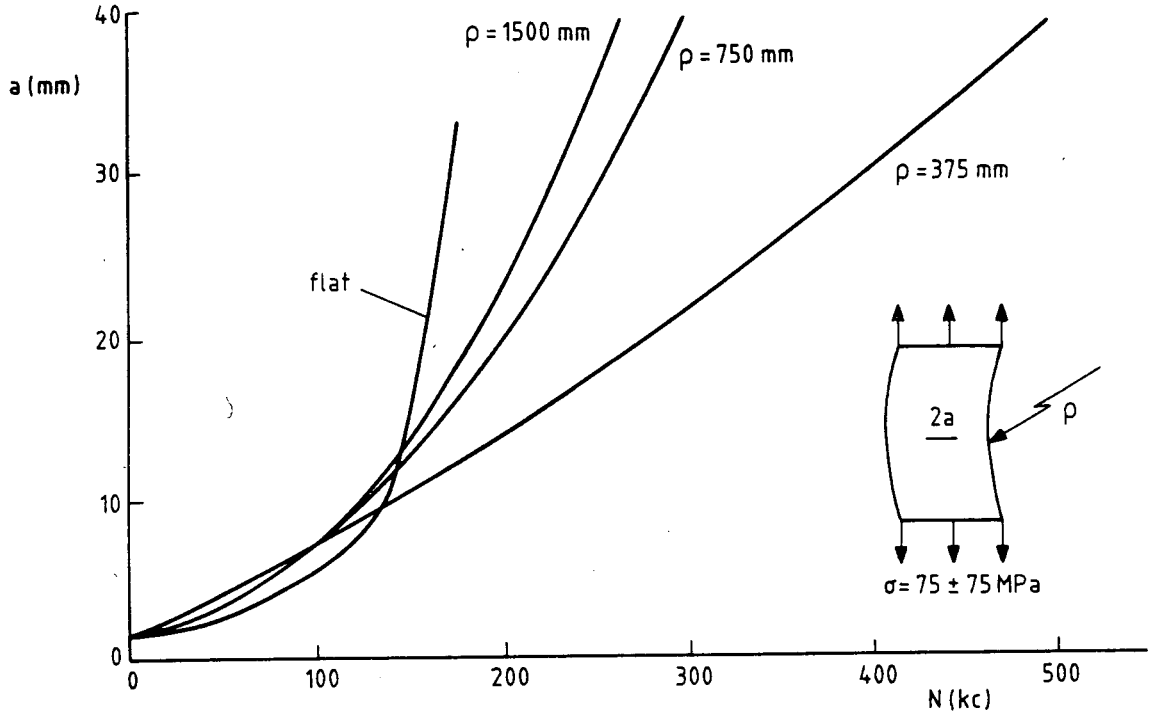

Figure 24a : ARALL 2H32

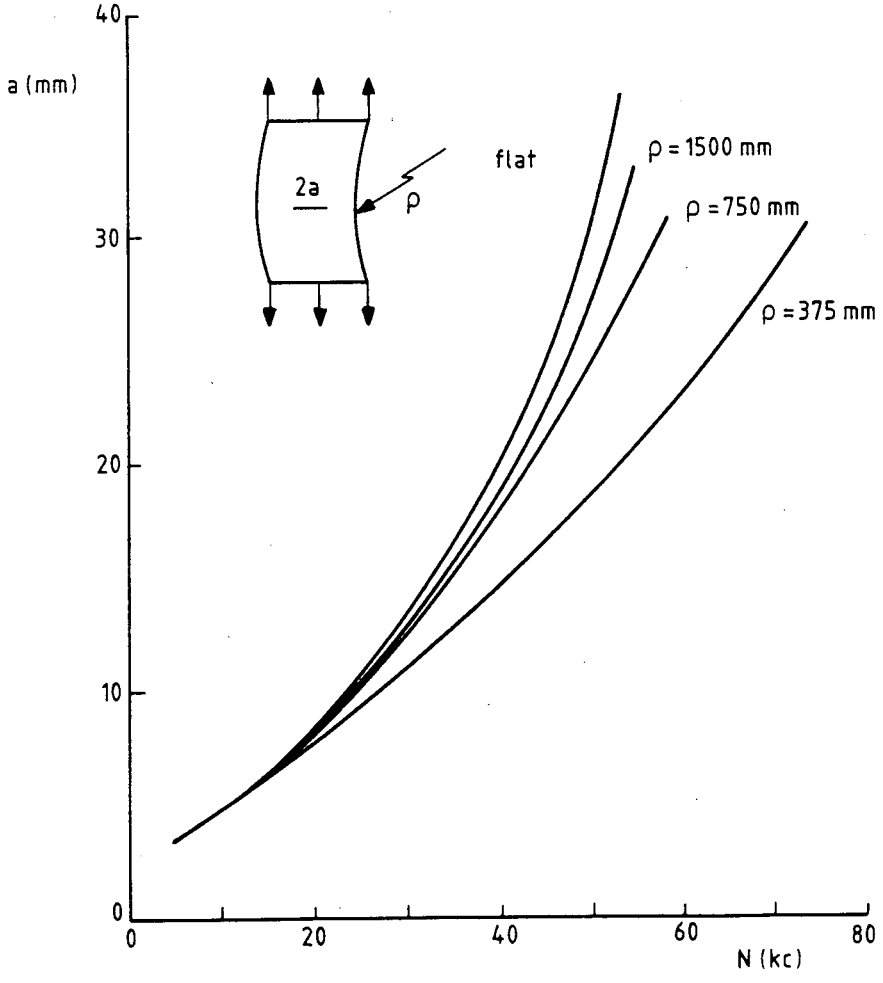

Figure 24b : ARALL 7H32

Figure 24 : CETS fatigue test results for ARALL (σ_{max} = 150 MPa, R = 0). Effect of curvature.

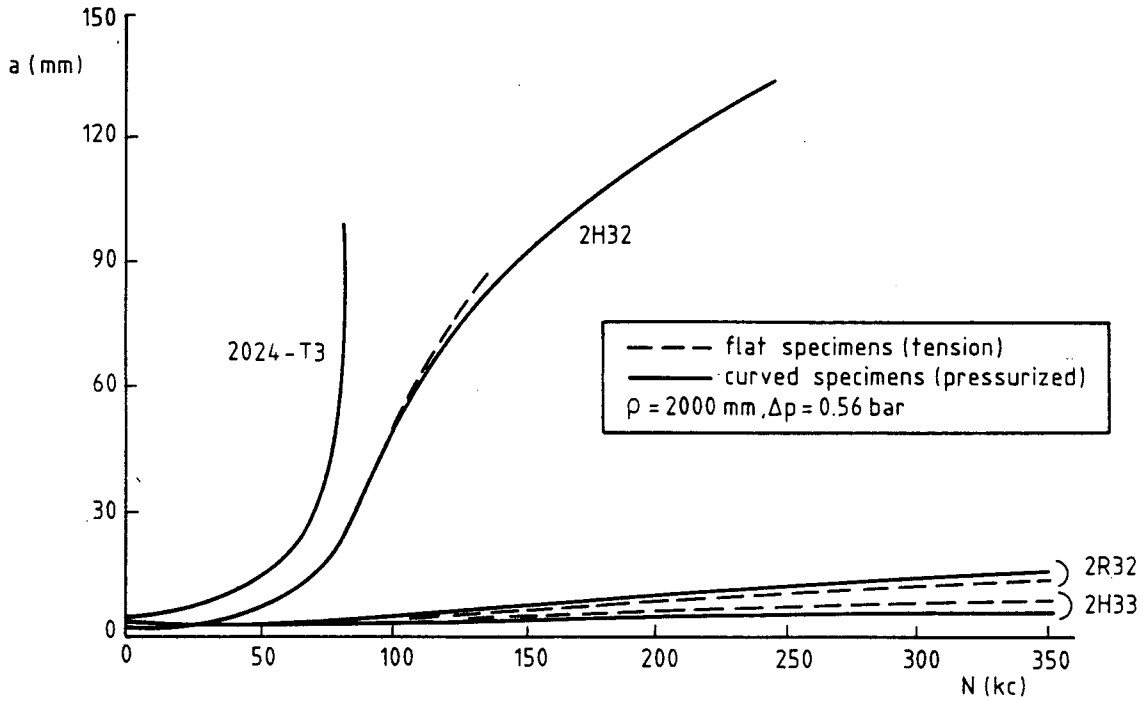

	t (mm)	σ_{hoop} (MPa)	$\sigma_{hoop} \cdot t$	γ (g/cm^3)	$\gamma \cdot t$	$\gamma \cdot t$ ratio
2024-T3	1.2	93.3	112	2.78	3.34	1
ARALL 2H32	0.82	136.6	112	2.41	1.98	0.59
ARALL 2H33	1.34	83.6	112	2.33	3.12	0.93
GLARE 2R32	0.91	123.1	112	2.58	2.34	0.70

Figure 25 : Fatigue crack growth in pressurized curved ARALL and GLARE panels Comparison to flat panels.